ANL/GTRI/TM-13/7

Preliminary Accident Analyses for Conversion of the University of Missouri Research Reactor (MURR) from Highly-Enriched to Low-Enriched Uranium

Nuclear Engineering Division

About Argonne National Laboratory

Argonne is a U.S. Department of Energy laboratory managed by UChicago Argonne, LLC under contract DE-AC02-06CH11357. The Laboratory's main facility is outside Chicago, at 9700 South Cass Avenue, Argonne, Illinois 60439. For information about Argonne and its pioneering science and technology programs, see www.anl.gov.

Availability of This Report

This report is available, at no cost, at http://www.osti.gov/bridge. It is also available on paper to the U.S. Department of Energy and its contractors, for a processing fee, from:

U.S. Department of Energy
Office of Scientific and Technical Information
P.O. Box 62
Oak Ridge, TN 37831-0062
phone (865) 576-8401
fax (865) 576-5728
reports@adonis.osti.gov

Disclaimer

This report was prepared as an account of work sponsored by an agency of the United States Government. Neither the United States Government nor any agency thereof, nor UChicago Argonne, LLC, nor any of their employees or officers, makes any warranty, express or implied, or assumes any legal liability or responsibility for the accuracy, completeness, or usefulness of any information, apparatus, product, or process disclosed, or represents that its use would not infringe privately owned rights. Reference herein to any specific commercial product, process, or service by trade name, trademark, manufacturer, or otherwise, does not necessarily constitute or imply its endorsement, recommendation, or favoring by the United States Government or any agency thereof. The views and opinions of document authors expressed herein do not necessarily state or reflect those of the United States Government or any agency thereof, Argonne National Laboratory, or UChicago Argonne, LLC.

ANL/GTRI/TM-13/7

Preliminary Accident Analyses for Conversion of the University of Missouri Research Reactor (MURR) from Highly-Enriched to Low-Enriched Uranium

prepared by

E. E. Feldman[1], L. P. Foyto[2], K. Kutikkad[2], J. C. McKibben[2],
N. J. Peters[2], J. G. Stevens[1], J. A. Stillman[1], and E. H. Wilson[1]
[1]GTRI Reactor Conversion Program, Nuclear Engineering Division, Argonne National Laboratory
[2]University of Missouri-Columbia Research Reactor

June 2013

This work is sponsored by the U.S. Department of Energy,
National Nuclear Security Administration Office of Global Threat Reduction (NA-21)

(This page intentionally left blank)

EXECUTIVE SUMMARY

This report contains the results of reactor accident analyses for the University of Missouri Research Reactor (MURR). The calculations were performed as part of the conversion from the use of highly-enriched uranium (HEU) fuel to the use of low-enriched uranium (LEU) fuel. The analyses were performed by staff members of the Global Threat Reduction Initiative (GTRI) Reactor Conversion Program at the Argonne National Laboratory (ANL) and the MURR Facility. The core conversion to LEU is being performed with financial support from the U. S. government.

In the framework of its non-proliferation policies, the international community presently aims to minimize the amount of nuclear material available that could be used for nuclear weapons. In this geopolitical context most research and test reactors, both domestic and international, have started a program of conversion to the use of LEU fuel. A new type of LEU fuel based on an alloy of uranium and molybdenum (U-Mo) is expected to allow the conversion of U.S. domestic high performance reactors like MURR. This report presents the results under a set of accident conditions for MURR cores fueled with HEU U-Al_x dispersion fuel or LEU monolithic U-Mo alloy fuel with 10 wt% Mo.

For the proposed LEU-fueled core, previous studies [1] have shown that in order to maintain the neutron flux and current levels at various crucial experimental locations within the reactor at the same level after the fuel conversion from the HEU to LEU, the steady-state operating power level must be increased from 10 MW to 12 MW. Hence the accidental positive reactivity insertions, and the loss of coolant and loss of flow accidents for the LEU core were initiated from an initial steady-state power level of 12 MW. It is noted that all references to the core power level for MURR are the *thermal* power output of the reactor (i.e., MW*t*).

Reactivity Insertion Accidents:

Accidents resulting from the uncontrolled or unanticipated insertion of positive reactivity in the MURR core have been evaluated to assess the impact of fuel conversion on reactor safety. The MURR Safety Analysis Report (SAR) [2] postulated three step reactivity insertion accidents and two continuous ramp reactivity insertion accidents. These were evaluated with version 5.0 of the PARET/ANL code [3] and shown to result in no damage to the core fueled with HEU.

The PARET/ANL model parameters employed in the MURR SAR were examined in detail and updated with appropriate values for both HEU and LEU fueled cores. Specifically, the PARET/ANL model was revised to utilize reactivity feedback coefficients, detailed power distributions, and control bank worths for the reactor safety system that were calculated for HEU and LEU fueled cores with a detailed MCNP5 [4] core model. Lastly, a more recently released version of the PARET/ANL code, version 7.5, was utilized for the current work.

Several core states were identified in Reference 1 to provide core power distributions for the steady-state thermal-hydraulic safety basis [5]. The most challenging of these core states were evaluated as steady-state reactor conditions for the initiation of the reactivity insertion accidents. In this preliminary accident analysis, the peak fuel temperatures in only fresh HEU and LEU fuel plates were evaluated. The evaluation of fuel temperatures in depleted plates resulting from reactivity insertion accidents will be conducted in Phase II of the analysis.

For the most limiting accident, which is a 0.006 $\Delta k/k$ step insertion of reactivity in a fresh critical core at full power, the peak HEU U-Al_x fuel meat temperature is calculated to be 444 ^{o}F (229 ^{o}C). The same accident is also the most limiting for the LEU fuel, resulting in a peak U-10Mo temperature of 500 ^{o}F

(260 ^{o}C). In both cases, the fuel temperature is well below the measured fuel blister threshold temperatures of 896 ^{o}F (480 ^{o}C) and 752 ^{o}F (400 ^{o}C) for HEU and LEU fuel, respectively.

Loss of Coolant and Loss of Flow Accidents:

The substantial RELAP5 code [6] model in the MURR SAR has been examined in significant detail. Improvements made as part of the current analysis included revising the reactor trip and protection system model; improving the detail of the hydraulic parameters of the HEU core model; and adjusting the thermal conductivity of the HEU fuel meat. In the models the core is represented by the single fuel element with the highest peaking factors and all coolant channels and fuel plates are explicitly represented. In the RELAP5 model this element has eight times the flow, flow area, heat transfer area, and power of a single element so as to represent the entire eight-element core. Each fuel plate is divided into four axial nodes. For the HEU model, the 10 MW core power distribution was set to represent element 7 of core power distribution 1B1, which is the element that has the highest heat flux in core 1B1 (i.e., the core loading with most challenging power distribution).

The LEU model was created by transforming the single-element HEU core model into the equivalent single-element LEU CD35 core model. For the LEU model, the 12 MW core power distribution was set to represent element 6 of core power distribution 5B1, which is the element that has the highest heat flux in core 5B1.

As is typical of this type of analysis, the models in the current work and in the SAR analysis represent best-estimate models in that they do not include additional engineering hot channel peaking factors and the transients are initiated from nominal full-power conditions.

In the current analysis a single unified HEU core model was used with only minor input changes to model two Loss of Coolant Accidents (LOCA) and one Loss of Flow Accident (LOFA). As described in the MURR SAR, these three events are the worst three potential primary coolant system accidents:

1) a cold-leg LOCA caused by a double-end break in the 12-inch diameter inlet piping outside of the pool boundary and downstream of inlet isolation valve 507B,
2) a hot-leg LOCA caused by a double-end break in the 12-inch diameter outlet piping outside of the pool boundary and upstream of outlet isolation valve 507 A, and
3) a LOFA caused by an 8-inch diameter breach in the 8-inch cold-leg piping at a flow control diaphragm valve located upstream of the cold-leg isolation valve.

In an analogous manner, a single unified core model was used to analyze the same three transients for the LEU core.

Key HEU results for each transient were compared with their LEU counterparts and their MURR SAR counterparts. In all cases, the peak fuel centerline temperature occurs at the scram or a few tenths of a second after it, and always during the first second of the transient. The MURR SAR analysis of the HEU core and the current analysis of the HEU and the LEU cores show that, as expected, the cold-leg LOCA causes the quickest reduction in flow through the core and consequently is the most limiting in that it produces the highest peak fuel centerline temperature of the three transients.

For the limiting transient, the cold-leg LOCA, the SAR shows that the fuel node that produces the highest transient temperature has an HEU fuel meat temperature rise of 68 °F (38 °C) from the initial steady-state value. This is to be compared with the 97 °F (54 °C) temperature rise in the HEU core predicted by the current analysis. The peak HEU fuel temperature during the LOCA is predicted to be 342 °F (172 °C). For the LEU core the fuel node that produces the highest transient temperature has a fuel meat

temperature rise of only 36 °F (20 °C), which is very modest for such a severe accident. The peak LEU fuel temperature during the LOCA is predicted to be 347 °F (175 °C).

Conclusions:

The preliminary results provided herein indicate acceptable thermal performance for the LEU core at 12 MW, and a reasonable comparison between the current and the MURR SAR results for the HEU core at 10 MW.

(This page intentionally left blank)

TABLE OF CONTENTS

EXECUTIVE SUMMARY ..... **i**

TABLE OF CONTENTS ..... **v**

List of Figures ..... **vii**

List of Tables ..... **viii**

1.0 INTRODUCTION **1**

2.0 REACTIVTY INSERTION ACCIDENTS **2**

2.1 Introduction 2
2.2 Modeling of Reactivity Insertion Accidents 2
2.3 Step Insertions of Positive Reactivity Accidents 5
2.3 Continuous Control Blade Withdrawal Accidents 13
2.3.1 Continuous Blade Withdrawal From Full Power 13
2.3.2 Startup Accident 14
2.4 Conclusions 16

3.0 LOSS OF COOLANT AND LOSS OF FLOW ACCIDENTS **17**

3.1 Background and Goals 17
3.2 Accidents to Be Considered 17
3.3 Model 22
3.3.1 Model as Provided in the MURR SAR 22
3.3.2 Recent Modifications to the MURR RELAP5 Model 22
3.3.2.1 RELAP5 Reactor Trip and Plant Protection System Model 22
3.3.2.2 Improved Core Channel Hydraulic Diameters, Laminar-Flow Friction Shape Factors, and Relative Roughness 26
3.3.2.3 Core Heat Transfer Areas and Nodal Structure 27
3.3.2.4 Secondary Sides Were Added to Primary and Pool Heat Exchangers 27
3.3.2.5 Fuel Thermal Properties 28
3.3.2.6 LEU and HEU Core Models 29
3.3.2.7 Unified Models 30
3.4 Results 31
3.5 Discussion 38
3.6 Conclusions 39

4.0 CONCLUSIONS **41**

REFERENCES **43**

Appendix A: Tables of Key HEU and LEU Core Parameter Data **45**

List of Figures

Figure 2.1. MURR Control Bank Worth Curves. 5
Figure 2.2. Power for HEU Core Step Reactivity Insertion Transients Without Scram in Core 1B1. 9
Figure 2.3. Power for HEU Core 0.006 Δk/k Step Insertion Transient: Effect of Reactor Scram. 10
Figure 2.4. Fuel Temperature for HEU Core 0.006 Δk/k Step Insertion Transient: Effect of Reactor Scram. 10
Figure 2.5. Power for LEU Core Step Reactivity Insertion Transients Without Scram in Core 5B1. 11
Figure 2.6. Power for LEU Core 0.006 Δk/k Step Insertion Transient: Effect of Reactor Scram. 12
Figure 2.7. Fuel Temperature for LEU Core 0.006 Δk/k Step Insertion Transient: Effect of Reactor Scram. 12
Figure 2.8. Power for 0.0003 Δk/k/sec Ramp Insertion of Reactivity. 13
Figure 2.9. Fuel Temperature for 0.0003 Δk/k/sec Ramp Insertion of Reactivity. 14
Figure 2.10. HEU Core Power During Simulation of Startup Accident. 15
Figure 2.11. LEU Core Power During Simulation of Startup Accident. 16
Figure 3.1. Simplified Schematic of MURR Primary System Loop (Normal Path). 18
Figure 3.2. Simplified Schematic of MURR Primary System Loop (LOFA Upset Path). 20
Figure 3.3. Simplified Schematic of MURR Primary System Loop (Hot-Leg LOCA Configuration). 21
Figure 3.4. Simplified Schematic of MURR Primary System Loop (Cold-Leg LOCA Configuration). 21
Figure 3.5. Trip 1: Core Outlet Pressure. 24
Figure 3.6. Trips 2 and 3: Primary Flow. 24
Figure 3.7. Trip 4: Core Inlet Pressure. 25
Figure 3.8. Trip 5: Core Pressure Drop. 25
Figure 3.9. Trip 7: Core Outlet Isolation Valve Starts to Close. 25
Figure 3.10. Trip 8: Core Inlet Isolation Valve Starts to Close. 26
Figure 3.11. Saturation Temperature of Water. 26
Figure 3.12. HEU Initial Fuel Centerline Temperatures. 32
Figure 3.13. LEU Initial Fuel Centerline Temperatures. 32
Figure 3.14. HEU Fuel Centerline Temperature History of Hottest Node. 33
Figure 3.15. LEU Fuel Centerline Temperature History of Hottest Node. 33
Figure 3.16. HEU Velocity in Channel 2 (between Plates 1 and 2). 35
Figure 3.17. LEU Velocity in Channel 23 (between Plates 22 and 23). 35
Figure 3.18. Coolant and Heat Transfer Conditions at the Limiting HEU Cold-Leg LOCA Node (Plate 2, Node 3). 37

List of Tables

Table 2.1. Key Reactor Parameters for Reactivity Insertion Accidents in the MURR SAR. 2
Table 2.2. Reactivity Feedback Coefficients and Kinetics Parameters for MURR Calculated with MCNP5. 3
Table 2.3. Thermo-Physical Properties of Materials in PARET/ANL Models. 4
Table 2.4. Key Reactor Parameters for Reactivity Insertion Accidents in Current Work. 5
Table 2.5. HEU Step Reactivity Insertion Transients. 7
Table 2.6. LEU Step Reactivity Insertion Transients. 8
Table 3.1. Key Reactor and Pool Parameters. 29
Table 3.2. Fuel Centerline Temperatures for the Fuel Node of the Peak. 34
Table A.1. HEU Core Coolant Channel Hydraulic Diameters, Shape Factors, and 8 × Flow Areas. 45
Table A.2. LEU Core Coolant Channel Hydraulic Diameters, Shape Factors, and 8 × Flow Areas. 46
Table A.3. HEU Fuel Plate Heat Transfer Areas for Flat-Plate (Rectangular) Geometry. 47
Table A.4. LEU Fuel Plate Heat Transfer Areas for Flat-Plate (Rectangular) Geometry. 48
Table A.5. Thermal Properties in MURR RELAP5 Models. 49

1.0 INTRODUCTION

The University of Missouri Research Reactor (MURR) is a multi-disciplinary research and education facility providing a broad range of analytical and irradiation services to the research community and the commercial sector. The source of neutrons for the experimental facilities of the MURR is a compact fuel region which has a fixed geometry consisting of eight fuel elements, each having identical physical dimensions. The fuel elements are placed vertically around an annulus between two cylindrical aluminum pressure vessels. The MURR is currently fueled with highly-enriched uranium (HEU) in an aluminide dispersion ($U\text{-}Al_x$) fuel.

In the framework of its non-proliferation policies, the international community presently aims to minimize the amount of nuclear material available that could potentially be diverted for nuclear weapons. In this geopolitical context, most research and test reactors, both domestic and international, have started a program of conversion to the use of low-enriched uranium (LEU) fuel. A new type of LEU fuel based on an alloy of uranium and molybdenum (U-Mo) is expected to allow the conversion of U.S. domestic high performance reactors like MURR.

Safety analyses of the MURR core fueled with a monolithic alloy of uranium and 10 wt% molybdenum (U-10Mo) were previously conducted to establish the steady-state safety basis of the reactor using the CD35 fuel element design [1, 5]. The thermal-hydraulic analyses of the reactor required detailed power distributions and geometrical considerations in order to identify regions of interest for safety analyses. In order to understand the impacts of accident and transient scenarios in a core fueled with an LEU U-10Mo element, a set of preliminary accident analyses have been performed. NUREG-1537 guidelines [7] postulate nine classes of postulated accident-initiating scenarios. The preliminary analyses include evaluation of those which have been the most challenging to fuel integrity including reactivity insertion accidents, loss of coolant accidents, and a loss of flow accident. The objective of these preliminary analyses is to determine the range of conditions and temperatures that the fuel, which is under development, should be expected to experience under off-normal and other transient scenarios.

2.0 REACTIVTY INSERTION ACCIDENTS

2.1 Introduction

Insertion of uncontrolled and/or unanticipated positive reactivity to either a critical reactor or during a reactor startup is one of the nine (9) postulated accident-initiating scenarios required to be analyzed for potential radiological consequence per the NUREG-1537 guidelines [7].

Following the guidance provided in NUREG-1537, in this section, two different accident scenarios for an insertion of positive reactivity were evaluated for the selected LEU core (CD-35) and the results are compared against those for the current HEU core. First, several positive step reactivity insertions, based upon the various maximum reactivity limits given in the MURR Technical Specifications (T.S), were considered. Second, a continuous ramp insertion of positive reactivity based on the simultaneous continuous withdrawal of MURR's four shim control blades was considered. The exact mechanisms or events that could cause these reactivity insertions can vary, but could include an inadvertent rapid insertion or removal of an experiment from the center test hole, reactor or equipment malfunction, or operator error. All the analyses in this section were performed using the PARET/ANL (V. 7.5) code [3]. PARET/ANL is a 1-dimensional reactor transient analysis code that models plate, pin, and nested tube fuel geometries.

2.2 Modeling of Reactivity Insertion Accidents

For the current HEU-fueled core, the accidental positive step reactivity addition accident scenarios were analyzed in the MURR SAR [2] from an initial steady-state power level of 10 MW, with coolant flow, pressure, and core inlet temperature conditions as specified in Table 2.1. Primary coolant temperature and void feedback coefficients corresponding to the MURR T.S. limits of -6.0×10^{-5} $\Delta k/k/^{o}F$ and -2.0×10^{-3} $\Delta k/k/\%$ void, respectively, were employed. Based on an effective delayed neutron fraction of 0.738%, the reactivity feedback coefficients were converted into units expected by PARET/ANL as -0.0146$/^{o}C and -0.271 $/%-void for the coolant temperature and void coefficients, respectively. The continuous ramp insertion of positive reactivity accident scenario was also analyzed from low power (1 W) and from a nominal steady-state power of 10 MW. In the MURR SAR, calculations were performed with version 5.0 of the PARET/ANL code.

Table 2.1. Key Reactor Parameters for Reactivity Insertion Accidents in the MURR SAR.

Parameter	Nominal Value	Assumed Value
Reactor Power	10 MW	10 MW
Primary Coolant Flow Rate	3,800 gpm	3,600 gpm
Reactor Core Inlet Pressure	75 psia	75 psia
Reactor Core Inlet Temperature	120 ^{o}F	130 ^{o}F

A review of the PARET/ANL models used in the MURR SAR analyses was conducted. The review found some modeling inconsistencies, including:

- The coolant properties of D_2O instead of H_2O were inadvertently used in the MURR SAR analyses. An evaluation of the impact of using the incorrect coolant properties showed that this has a negligible impact on the predicted peak power for the most limiting transient of a step reactivity insertion of 0.006 $\Delta k/k$; the impact on the peak power was +0.002 MW out of a predicted peak power of 34.356 MW.
- The coolant flow direction was specified as upflow through the core rather than downflow. Again, the impact of this modeling error was assessed. Specifying coolant upflow rather than coolant downflow increases the predicted peak power for the 0.006 $\Delta k/k$ reactivity insertion transient by +0.023 MW.

- The primary coolant temperature coefficient of -6.0 x 10^{-5} $\Delta k/k/^{o}F$ specified by the MURR T.S. includes the effects of both coolant temperature and density, which is the typical definition for the coolant temperature coefficient in reactor operations. However, in PARET/ANL, the coolant temperature coefficient is assumed to include only the reactivity feedback associated with changes in the water temperature. The reactivity feedback due to a change in water density due to water temperature changes is accounted for in the primary coolant void coefficient. Consequently, directly using the MURR T.S. value for the coolant temperature coefficient in PARET/ANL will result in too much negative reactivity feedback.

In the current analysis, the first two modeling inconsistencies identified above have been corrected in the PARET/ANL models. Furthermore, instead of using any MURR T.S. value for the reactivity feedback coefficients, the reactivity feedback coefficients and reactor kinetics parameters (effective delayed neutron fraction, β_{eff}, and neutron lifetime, Λ) were calculated for the MURR core loaded with HEU or LEU fuel using an MCNP5 [4] core model. The coolant void, coolant temperature, and fuel temperature reactivity coefficients were calculated by making small perturbations to the appropriate reactor conditions from the nominal (hot operating) conditions in MCNP5. The kinetics parameters were calculated using the kinetics option in MCNP5. The validation of this methodology for calculating the feedback coefficients is described in more detail Section 4.5 of Reference 1.

The reactivity coefficients and kinetics parameters were calculated for three core loadings of each fuel type (HEU or LEU): all fresh fuel, a typical mixed burnup core loading at beginning-of-cycle (BOC) with no xenon, and a typical mixed burnup core loading at equilibrium xenon conditions. For each fuel type, the smallest magnitude value calculated for each parameter was chosen for the current work, which is the conservative approach. Table 2.2 summarizes the reactivity feedback coefficients used in the current work.

Table 2.2. Reactivity Feedback Coefficients and Kinetics Parameters for MURR Calculated with MCNP5.

Parameter	**HEU**	**LEU**
Coolant Density Coefficient, \$/%-void	-0.301 ± 0.011	-0.304 ± 0.011
Coolant Temperature Coefficient, $\$/^{o}C$ (Note: Temperature only)	-5.25 x 10^{-3} ± 9.4 x 10^{-5}	-1.63 x 10^{-3} ± 9.5 x 10^{-5}
Fuel Temperature Coefficient, $\$/^{o}C$	N/A	-0.911 x 10^{-3} ± 5.2 x 10^{-5}
β_{eff}	0.783% ± 0.003%	0.765% ± 0.002%
Λ (μs)	49.5 ± 0.10	38.7 ± 0.03

PARET/ANL is a 1-dimensional code that models a fuel plate and its associated coolant during the reactor transient. The construction of fuel meat, clad, and coolant are termed a "channel." Both "average" and "peak" channels are typically represented in the model, with the average channel representing the bulk of the core and the peak channel representing that plate which is expected to reach the highest temperature as a result of the transient. There is no heat transfer between the channels in PARET/ANL, but the channels are coupled through reactivity feedback effects; that is, the reactivity feedbacks from each channel in the model are volume-weighted and summed to compute the total core reactivity and power as a function of time in the transient.

Detailed, 3-dimensional power distribution data in MURR cores loaded with HEU or LEU fuel were calculated in Reference 1 using MCNP5. For the average channel in the PARET/ANL models, the 24-

node axial peaking factors were calculated for the average of all plates in the core. For the peak channel, the 24-node axial peaking factors were calculated for the plate and azimuthal strip in the core that generated the highest local heat flux. In this preliminary phase of the accident analyses, only fresh fuel plates were considered for assessing the peak transient conditions. In the Phase II analysis, the impact of fuel burnup, oxide layer growth, and coolant channel restriction due to oxide growth and fuel creep on the accident results will be assessed.

The materials represented in the PARET/ANL model are the fuel meat, clad, and water. The coolant properties are generated by the code using built-in functions, while the thermal conductivity and specific heat of the fuel meat and clad are supplied by the user. For the HEU fuel and Al clad, the thermal conductivities utilized for the steady-state thermal-hydraulic safety basis [5] were used. For the specific heat of the aluminide fuel and Al clad, the values from the MURR SAR model were used. For the U-10Mo monolithic alloy, functional representations of the thermal conductivity and specific heat from Reference 8 were used. Only fresh fuel properties were considered in this preliminary accident analysis. As stated above, the impact of fuel burnup will be addressed in Phase II. The material properties used in the PARETN/ANL models in this work are summarized in Table 2.3.

Table 2.3. Thermo-Physical Properties of Materials in PARET/ANL Models.

	Thermal Conductivity (W/m-K)	**Specific Heat (J/m^3-K)**
HEU aluminide fuel	40.0	2.36E+06
U-10Mo alloy	10.2 + 0.0351•T, where T is the fuel temperature in ^{o}C	2.33E+06 + 871•T + 0.339•T^2, where T is the fuel temperature in ^{o}C
Al-6061	150.0	2.48E+06

External reactivity control of the MURR core is accomplished with four Boral© shim blades that move in a water-filled gap between the reactor outer pressure vessel and the beryllium reflector. When any one of the various reactor trip settings is reached, a scram signal is sent and the blades are dropped to insert a sufficiently large amount of negative reactivity and terminate the transient. There is a short delay time of 150 milliseconds from the time the scram signal is sent to the start of blade motion.

The reactivity worth of the entire control bank was calculated with MCNP5 for HEU-fueled and LEU-fueled cores under different core burnup conditions. The calculated control bank worth curves are provided in Figure 2.1. For this preliminary phase of the accident analyses, only fresh blades were considered. The control bank worth for the LEU-fueled cores is about $4 less than for the HEU-fueled cores, but the total bank worth is still sufficiently large to compensate for the credible reactivity insertion accidents postulated for MURR. The reactivity worth as a function of time from the beginning of the blade drop (assuming a blade drop rate of 0.76 m/s) was calculated and entered in the PARET/ANL models.

The control blade withdrawal rate in MURR is 1 inch/minute. Using the control bank worth curves in Figure 2.1 and the blade withdrawal rate, the calculated maximum reactivity insertion from control bank withdrawal is 0.00027 Δk/k/s for HEU-fueled cores and 0.00023 Δk/k/s for LEU-fueled cores. These values are less than 0.00030 Δk/k/s, which is the MURR T.S. limit on the reactivity insertion from control bank withdrawal.

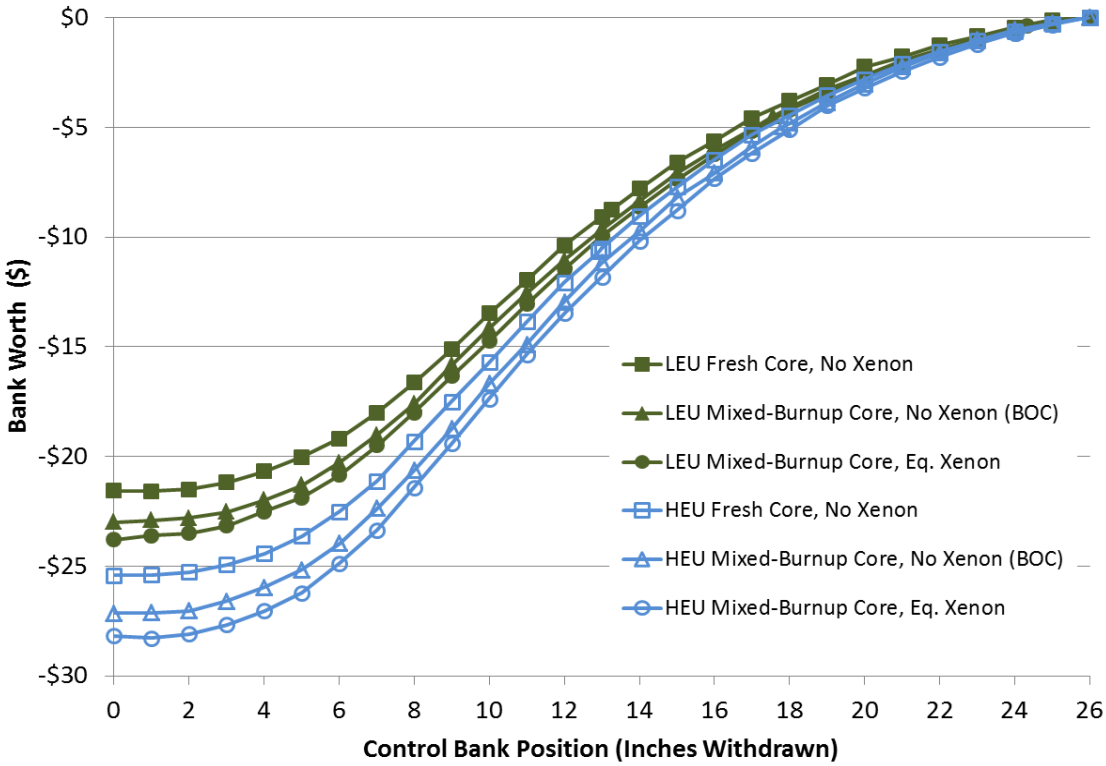

Figure 2.1. MURR Control Bank Worth Curves.

Table 2.4 summarizes the initial steady-state power level, coolant flow, pressure, and core inlet temperature conditions at the initiation of the reactivity insertion accidents analyzed in the current work. For the proposed LEU-fueled core, previous studies have shown [1] that in order to maintain the neutron flux and current levels at various crucial experimental locations within the reactor at the same level after the fuel conversion from the HEU to LEU, the steady-state operating power level must be increased from 10 MW to 12 MW. Hence the accidental positive reactivity insertions for the LEU core were initiated from an initial steady-state power level of 12 MW.

Table 2.4. Key Reactor Parameters for Reactivity Insertion Accidents in Current Work.

Parameter	HEU	LEU
Steady-State Reactor Power	10 MW	12 MW
Primary Coolant Flow Rate	3,600 gpm	3,600 gpm
Pressurizer Pressure[1]	75 psia	75 psia
Reactor Core Inlet Temperature	130 ^{o}F	130 ^{o}F

[1]LSSS condition.

2.3 Step Insertions of Positive Reactivity Accidents

From the various reactivity limits given in the MURR T.S, three cases were selected for analyzing step reactivity insertions. These cases were selected since they bound all other potential accident initiating scenarios involving inadvertent positive reactivity insertions. The three cases analyzed are:

a) A positive step reactivity insertion of 0.0060 Δk/k, which is the maximum allowed absolute reactivity worth of all experiments in the center test hole; or the maximum allowed worth of each secured removable experiment; or the sum of the reactivity worths of all unsecured experiments installed in the reactor.

b) A positive step of 0.0025 Δk/k, which is the maximum allowed absolute reactivity worth of each individual unsecured experiment in the reactor.
c) A positive step of 0.0010 Δk/k, which is the maximum allowed absolute reactivity worth of each individual movable experiment in the reactor.

For both the current HEU fuel and proposed LEU fuel, several core states were evaluated. These core states were chosen based on the expected fuel burnup conditions (all fresh, mixed-burnup), xenon concentration, center flux trap contents, and control blade composition (fresh/depleted) and position (banked or skewed), all of which affect the peak local heat flux and hot-stripe heat flux in the core at the initiation of the transient. The rationale behind choosing these core conditions and the impact on the core power distribution are discussed in more detail in Section 4.2 of Reference 1. The HEU and LEU core states considered in the current work are listed below. All reactor transients were initiated from a critical condition and, unless specified otherwise, the flux trap was assumed to be loaded with typical samples for MURR operations and the control blades were fresh and banked.

- HEU Cores:
  - All fresh fuel core loading at BOC (1A)
  - All fresh fuel at BOC with empty flux trap and depleted/skewed control blades (1B1)
  - Typical mixed burnup core loading at BOC (3A)
  - Typical mixed burnup core at BOC with empty FT and depleted/skewed control blades (3B2)
  - Typical mixed burnup core with equilibrium xenon (4A)

- LEU Cores:
  - All fresh fuel core loading at BOC (5A)
  - All fresh fuel at BOC with empty flux trap and depleted/skewed control blades (5B1)
  - Typical mixed burnup core loading at BOC (7A)
  - Typical mixed burnup core with equilibrium xenon (8A)
  - Typical mixed burnup core with equilibrium xenon, empty FT, and depleted/skewed control blades (8A2)

Tables 2.5 and 2.6 summarize the steady-state conditions, accident conditions, and peak power and temperatures reached during the transient for the HEU and LEU cases analyzed. For the cases analyzed, the cores 1B1 for the HEU fuel and 5B1 for the LEU fuel, which have the highest local heat flux at steady-state, were found to result in the highest fuel temperatures in the transients that were evaluated.

Figure 2.2 shows the result of the various positive step reactivity insertions for the current HEU-fueled critical reactor from an initial steady-state power level of 10 MW. As expected, a positive step reactivity insertion will result in an initial power burst, which, for the 0.006 Δk/k step, is much higher than the steady-state safety limit power level for the reactor under the assumed operating pressure, coolant inlet temperature and flow conditions. Increased coolant temperature and core voiding are the major negative reactivity feedback mechanisms for the HEU core. These feedback mechanisms will halt the rapid power escalation following a positive reactivity step insertion. Thus, the initial power burst lasts for only a few hundred milliseconds before the inherent feedback mechanisms act to limit further power increase. Subsequently, if no automatic action is taken by the reactor safety system, the power will continue to rise following the initial power burst until a new steady-state burnup power level is reached.

Table 2.5. HEU Step Reactivity Insertion Transients.

Initial Conditions (unless specified different below):

10 MW — Flow = 3600 gpm

T_{inlet} = 54.4 C (130 F) — Pressurizer Pressure = 75 psia (63.7 psia at core inlet)

			Steady-state								Transient			
					Hot Plate			Average Plate						
Accident Type	Reactivity Insertion	Core	Hot Stripe Heat Flux (W/cm^2)	Peak Local Heat Flux (W/cm^2)	T_{outlet} (C)	$T_{clad\text{-}surf,max}$ (C)	$T_{fuel,max}$ (C)	T_{outlet} (C)	$T_{clad\text{-}surf,max}$ (C)	$T_{fuel,max}$ (C)	P_{peak} (MW)	T_{outlet} (C)	$T_{clad\text{-}surf,peak}$ (C)	$T_{fuel,peak}$ (C)
All unsecured experiments	0.60% Δk/k ($0.77)	3A	131.25	185.27	80.58	114.56	124.97	66.07	83.08	87.77	33.66	139.66	189.33	224.34
		4A	125.45	167.97	79.34	109.91	119.48	66.03	80.42	84.59	33.52	131.35	186.05	216.01
		1A	126.81	181.40	79.63	113.86	124.08	66.09	85.42	90.62	34.42	139.52	189.72	225.05
		3B2	141.33	189.94	82.56	117.63	128.39	66.06	82.55	87.08	33.63	145.04	189.96	225.18
		1B1	139.16	197.57	82.17	119.78	131.01	66.09	84.77	89.80	33.93	147.00	191.30	**229.44**
		1B1/ SCRAM									33.75	128.05	188.97	223.29
Any unsecured experiment	0.25% Δk/k ($0.32)	1B1									15.44	96.79	151.04	168.38
Any moveable experiment	0.10% Δk/k ($0.128)	1B1									11.69	86.62	129.55	142.68

Table 2.6. LEU Step Reactivity Insertion Transients.

Initial Conditions (unless specified different below):

12 MW — Flow = 3600 gpm

T_{inlet} = 54.4 C (130 F) — Pressurizer Pressure = 75 psia (63.7 psia at core inlet)

			Steady-state								**Transient**			
					Hot Plate			Average Plate						
Accident Type	Reactivity Insertion	Core	Hot Stripe Heat Flux (W/cm^2)	Peak Local Heat Flux (W/cm^2)	T_{outlet} (C)	$T_{clad\text{-}surf,max}$ (C)	$T_{fuel,max}$ (C)	T_{outlet} (C)	$T_{clad\text{-}surf,max}$ (C)	$T_{fuel,max}$ (C)	P_{peak} (MW)	T_{outlet} (C)	$T_{clad\text{-}surf,peak}$ (C)	$T_{fuel,peak}$ (C)
All unsecured experiments	0.60% Δk/k ($0.78)	7A	130.63	210.77	77.50	122.00	142.92	65.95	86.82	96.73	42.16	130.11	191.70	252.29
		8A	148.97	192.95	80.66	118.70	137.92	65.90	83.42	92.26	42.04	136.04	189.46	242.17
		5A	125.27	222.22	73.91	123.73	145.61	65.96	89.21	99.90	42.25	116.96	192.22	254.48
		8A2	156.76	196.67	81.92	120.28	139.42	65.89	83.42	92.21	42.03	139.97	189.78	243.34
		5B1	133.75	234.01	77.48	128.08	150.93	65.96	88.43	98.84	42.21	130.11	193.54	**260.11**
		5B1/ SCRAM									42.21	118.39	193.54	259.46
Any unsecured experiment	0.25% Δk/k ($0.33)	5B1									18.76	89.92	164.80	198.11
Any moveable experiment	0.10% Δk/k ($0.131)	5B1									14.11	81.23	139.71	165.97

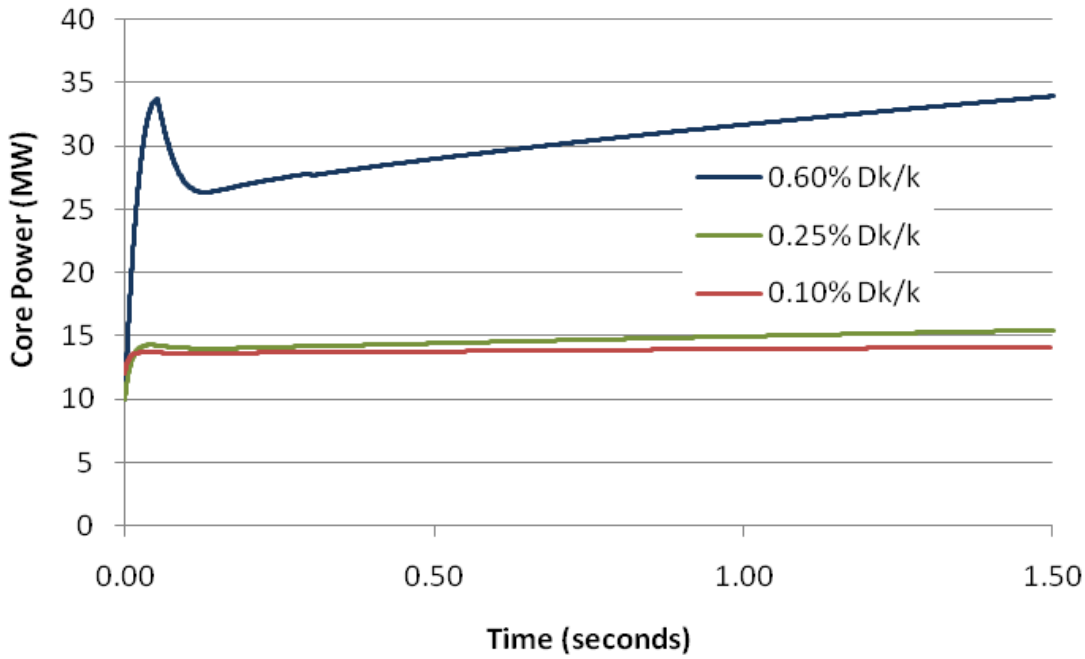

Figure 2.2. Power for HEU Core Step Reactivity Insertion Transients Without Scram in Core 1B1.

As a general principle, during rapid reactor transients a reactor can handle power bursts that are much higher than the steady-state burnout power level, since these power bursts last only for a few tenths of a second. It is only during steady-state operation or slow transients at power levels above the safety limit curves that melting of the fuel plate may result from a boiling "crisis" such as Departure from Nucleate Boiling or Flow Instability. To cause fuel damage during a rapid transient, the product of power level and time must yield enough total energy to reach the melting temperature of a fuel plate. Such reactor behavior has been conclusively shown by hundreds of power excursion tests performed at the Special Power Excursion Reactor Test (SPERT) facility at the National Reactor Testing Station in Idaho [9].

Figure 2.3 shows the effect of an automatic reactor scram terminating the most severe transient (0.006 Δk/k step). These automatic scrams are initiated by the reactor safety system either on short reactor period or high power and typically have a delay time of only a few hundred milliseconds. Experimental data indicate that either one of two short period or one of three high power trips in the MURR safety system will initiate a reactor scram within 150 milliseconds after the scram set point is reached, and sufficient redundancy in instrumentation exists to ensure that a post burst scram will occur. Calculated control blade worth and measured drop time data enabled the modeling of a reactor scram after the step insertion by PARET/ANL. Figure 2.3 shows reactor power behavior for the 0.006 Δk/k step insertion case after the initiation of a scram 150 milliseconds after the reactor power has exceeded the high-power trip setting of 12.5 MW (125% of full power).

Figure 2.4 shows the fuel centerline temperature for the 0.006 Δk/k step insertion case. The peak temperature reached during the 0.006 Δk/k step insertion is 229.4 ^{o}C, and the maximum clad surface temperature attained is 191.3 ^{o}C (Case 1B1). These values are much lower than the measured blister threshold temperature of 480 ^{o}C (896 ^{o}F) for the aluminide fuel [10]. As expected, the lower step reactivity insertions of 0.0025 Δk/k and 0.001 Δk/k result in much lower peak power bursts and peak fuel and clad surface temperatures.

Figures 2.3 and 2.4 clearly demonstrate that a scram after the postulated transients will safely shut down the reactor with no fuel damage occurring.

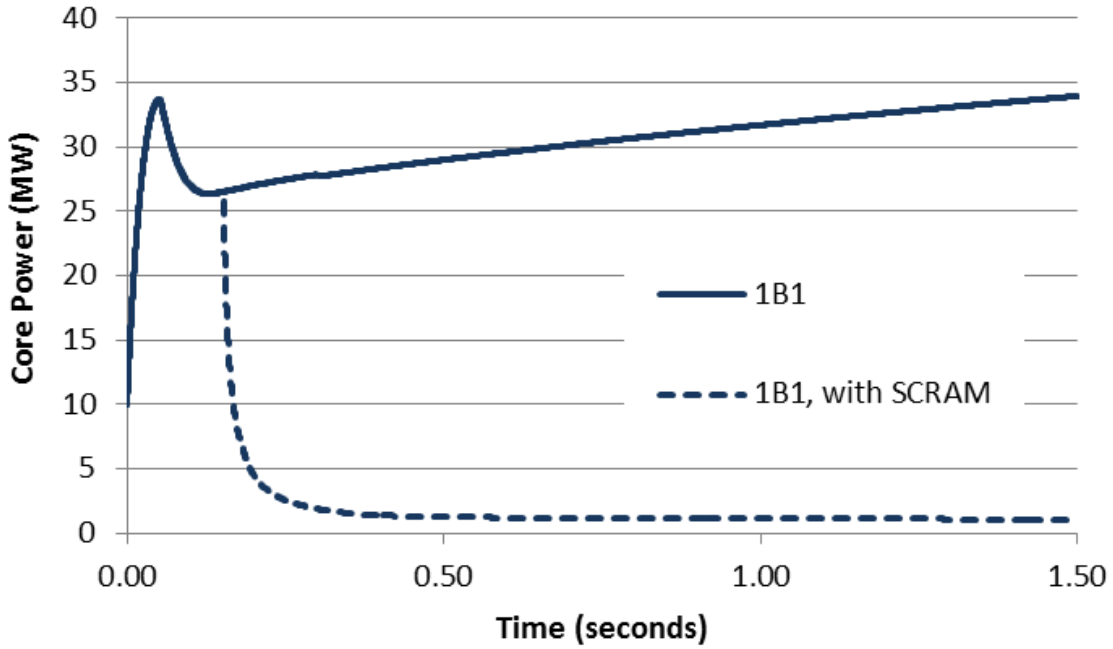

Figure 2.3. Power for HEU Core 0.006 Δk/k Step Insertion Transient: Effect of Reactor Scram.

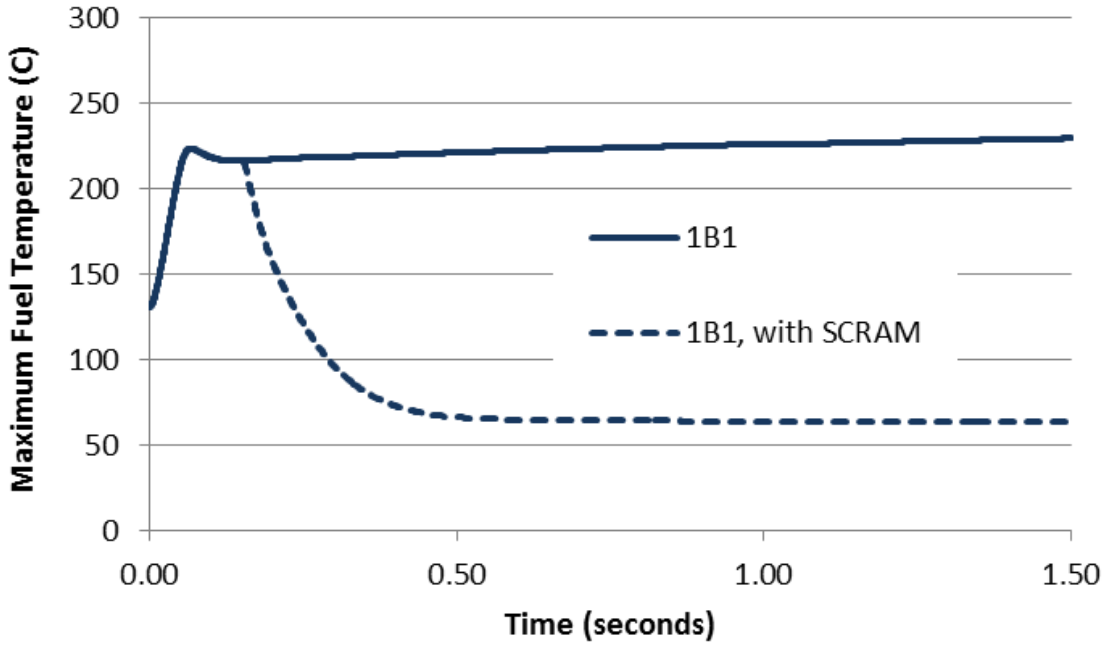

Figure 2.4. Fuel Temperature for HEU Core 0.006 Δk/k Step Insertion Transient: Effect of Reactor Scram.

In order to evaluate the impact of fuel conversion to LEU, the responses of the selected LEU-fueled core to the same set of positive step reactivity insertions were analyzed using the same methodology. Core inlet temperature, pressurizer pressure, and flow rates were kept the same as those for the HEU core. However, as mentioned earlier, for the LEU core the transients were initiated from a steady-state core power level of 12 MW. Furthermore, the reactivity feedback coefficients and control blade worth curves calculated for the LEU-fueled cores were employed in the PARET/ANL model. For the LEU-fueled core, in addition to the coolant temperature and density reactivity feedback effects, the inherent negative Doppler coefficient also aids in limiting the transient. Figure 2.5 shows the responses of the LEU core to various positive step reactivity insertions. As can be seen from the LEU core response, the initial higher steady-state power level and changes to the reactivity feedback coefficients result in a higher peak power burst compared to the HEU core – 42.2 MW for LEU from 12 MW compared to 33.9 MW for HEU from 10 MW.

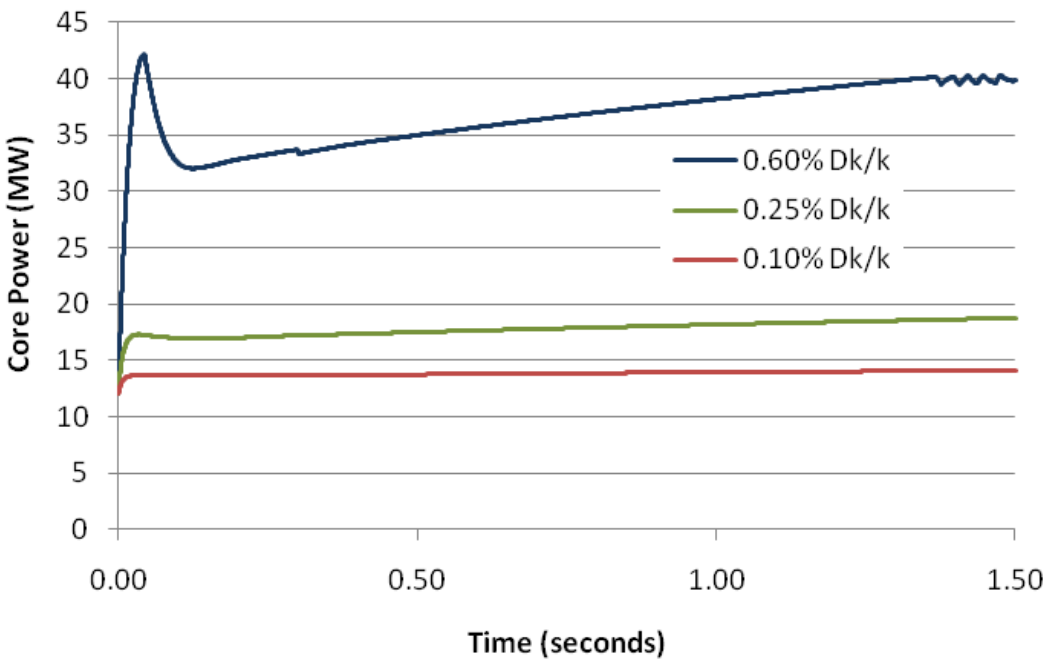

Figure 2.5. Power for LEU Core Step Reactivity Insertion Transients Without Scram in Core 5B1.

Similar to the HEU case, the automatic reactor protective system is designed to terminate the transient in the LEU core before the steady-state burnout power level is reached. Figure 2.6 presents the results of the 0.006 Δk/k step insertion accident in the limiting LEU core 5B1 assuming a high-power level trip point of 15 MW (125% of full power). The scram begins 150 milliseconds after the core power level reaches 15 MW. Figure 2.7 illustrates that the peak fuel temperature reached during the transient is 260.1 ^{o}C, well below the measured blister threshold temperature for depleted U-10Mo fuel of 400 ^{o}C (752 ^{o}F) for the proposed monolithic LEU fuel type [11].

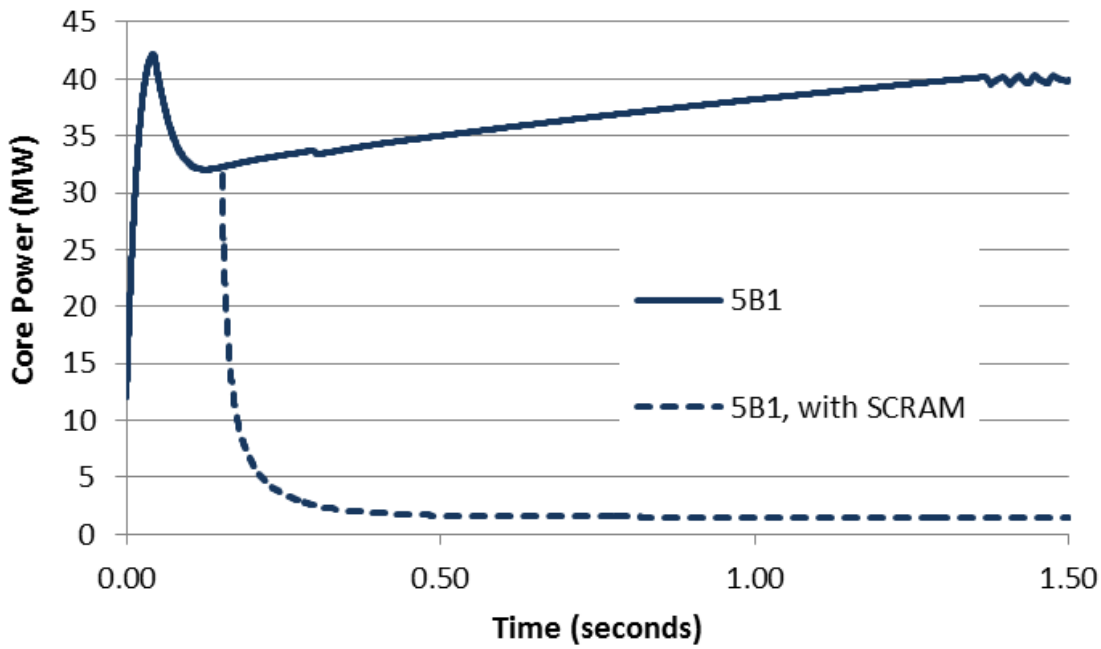

Figure 2.6. Power for LEU Core 0.006 Δk/k Step Insertion Transient: Effect of Reactor Scram.

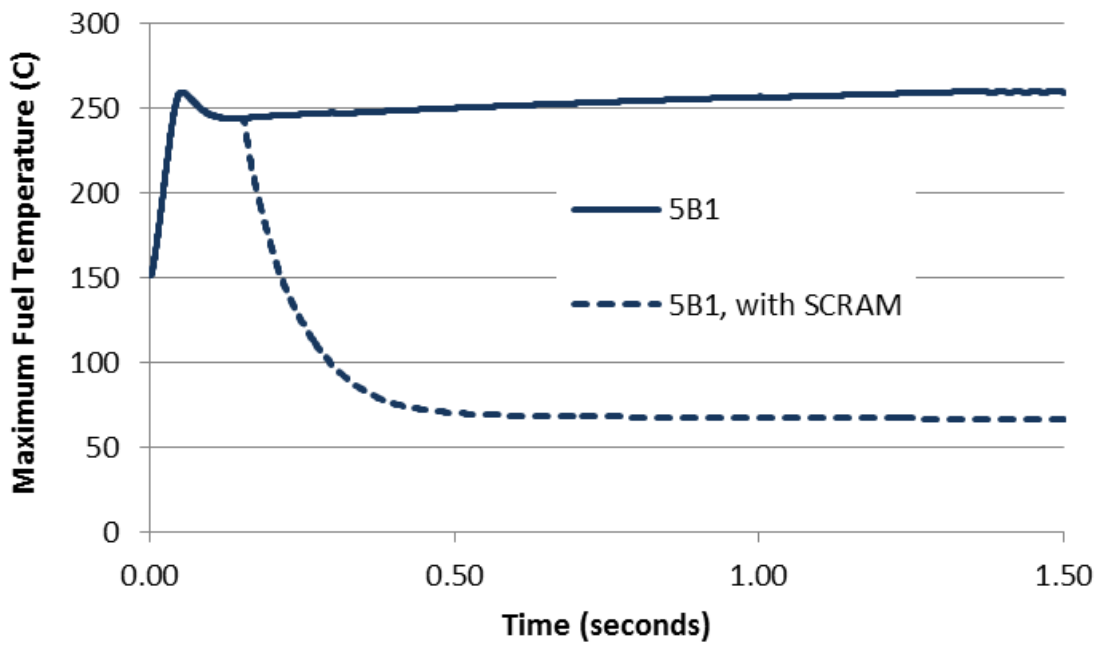

Figure 2.7. Fuel Temperature for LEU Core 0.006 Δk/k Step Insertion Transient: Effect of Reactor Scram.

2.3 Continuous Control Blade Withdrawal Accidents

The second class of reactivity accidents analyzed to assess the impact of fuel conversion is the continuous rod withdrawal accident. To be conservative, even though the reactivity addition resulting from the simultaneous withdrawal of all four shim control blades follows the typical differential rod worth curve behavior (with reduced worths at the beginning and at the end of rod withdrawal), the maximum value allowed by the MURR T.S. was imposed during the entire accident. Thus, a positive ramp reactivity insertion at the rate of 0.0003 Δk/k/sec, was considered.

Two subsets are considered within this class of accident. First a continuous simultaneous withdrawal of all four shim control blades while the reactor is operating at full power level (10 MW for HEU and 12 MW for LEU) has been analyzed. Second, an unanticipated continuous withdrawal of all control blades with no operator intervention during a reactor startup from low power levels is evaluated.

2.3.1 Continuous Blade Withdrawal From Full Power

The response of the HEU and the LEU cores to the ramp insertion while at full power is given in Figures 2.8 and 2.9. The behavior of the proposed LEU core is very similar to the current HEU core following a continuous shim blade withdrawal from a critical full power state. As expected, the higher initial steady-state power level and high-power trip point of the LEU core results in a higher power level prior to the initiation of reactor scram by the reactor safety system. The maximum power level reached for the LEU core is 15.2 MW compared to 12.6 MW for the HEU core. The peak fuel temperature reached during the transient is 149.1 ^{o}C for the HEU core, and 175.7 ^{o}C for the LEU core. These temperatures are well below the measured fuel blister threshold temperatures for the current aluminide fuel and the proposed monolithic fuel.

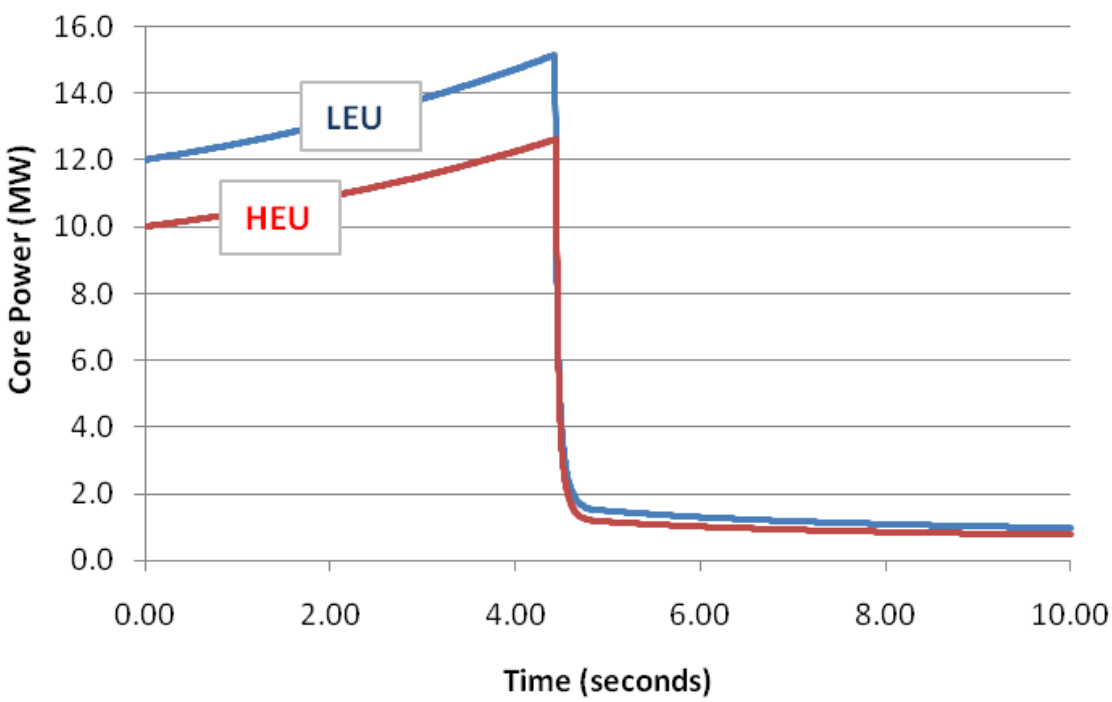

Figure 2.8. Power for 0.0003 Δk/k/sec Ramp Insertion of Reactivity.

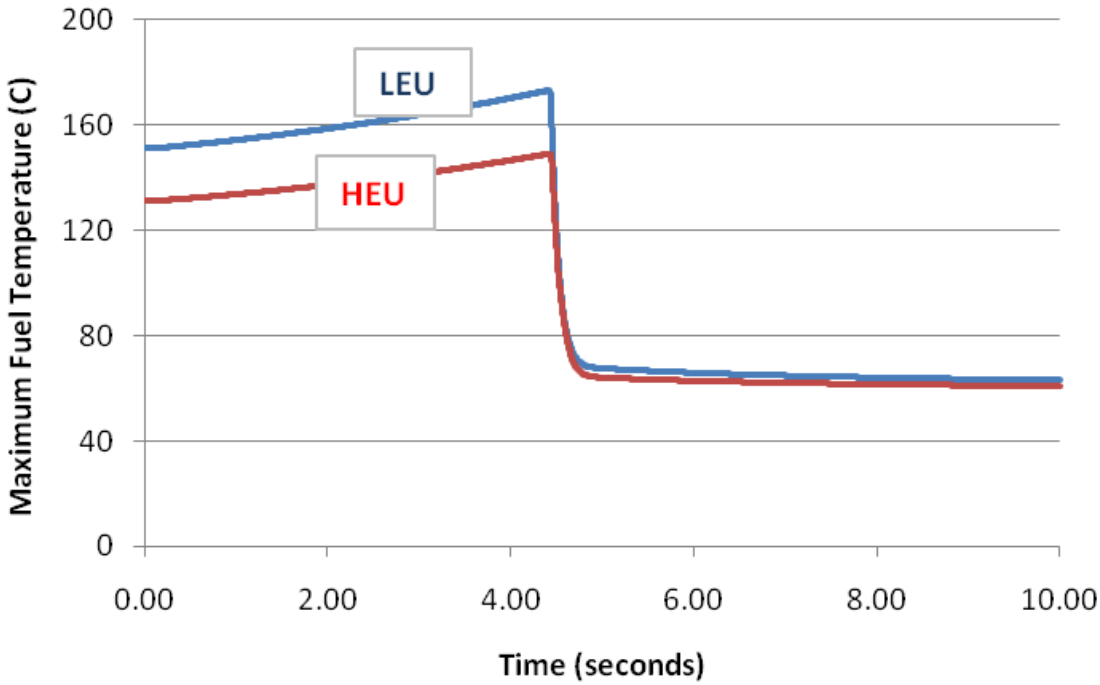

Figure 2.9. Fuel Temperature for 0.0003 Δk/k/sec Ramp Insertion of Reactivity.

2.3.2 Startup Accident

A second type of ramp reactivity insertion accident that has the potential for creating conditions that can lead to core damage is the startup accident. Typical reactor startups are very controlled evolutions with the blade withdrawal done in small incremental steps. Also, blade withdrawal is stopped at various predetermined control blade heights prior to reaching the critical control blade position for taking core multiplication data.

The startup accident postulates that all the control blades are withdrawn simultaneously (in gang) until the reactor passes through the critical state without any automatic or manual (operator) action to halt the uncontrolled blade withdrawal. Once the reactor passes through the critical state, the power increase is very rapid during such a transient. Furthermore, since the power level remains extremely low during the majority of the transient, no major reactivity feedback mechanisms exist to affect the reactor behavior, except for during the very end of the transient. The entire reactivity effect seen by the core is due to the withdrawal of the control blades.

To compare the impact of fuel conversion on such a transient, a startup accident was analyzed under similar conditions for both the HEU and LEU cores. A positive ramp reactivity insertion at the rate of 0.0003 Δk/k/sec, corresponding to the MURR T.S. limit on the maximum rate of reactivity insertion for all four shim control blades operating simultaneously, was introduced, starting with a subcritical power level of 1.0 W and a shutdown reactivity value of negative 0.042 Δk/k.

Figures 2.10 and 2.11 show the behavior of the reactor power due to this positive ramp reactivity insertion during a total transient time of 150.0 seconds (2.5 minutes) for HEU and LEU cores, respectively. It should be noted that even though the starting power level is the same for both the cores, the protective scram set point for the two cores will be different. For the current HEU core a high-power scram is

initiated once the reactor power level exceeds 12.5 MW, but for the LEU core that set point will be 15 MW.

For the HEU-fueled core, approximately 140 seconds into the transient, the reactor passes through the critical state. At this time, the reactor power level is approximately 16 W with a reactor period of approximately 11.4 seconds. Once the reactor passes through critical state, the increase in power is very rapid. At 150.0 seconds after initiation of the transient (ten seconds after passing through the critical state), the reactor power level exceeds 58 W with a reactor period of only 4.9 seconds. Sometime before this point, one of the two (or both) short period reactor safety trips, with a trip set point of 8.0 seconds, will act to terminate the transient.

For the LEU-fueled core, the reactor also reaches the critical state approximately 140 seconds after the commencement of the startup accident. At this time, the reactor power level is approximately 17 W with a reactor period of 10.5 seconds. Ten seconds after passing through the critical sate, the reactor power level is just over 60 W with a reactor period of 4.8 seconds. Just as for the HEU core, the two short period reactor safety trips will act to terminate the transient before this point is reached.

It should be noted that for both the HEU and LEU cores in the startup accident, the fuel temperature undergoes a negligible temperature increase due to the extremely low power level of the core before the transient is terminated. Because of the assumed conditions of coolant temperature and flow in this accident, the fuel temperature remains at 54.4 ^{o}C.

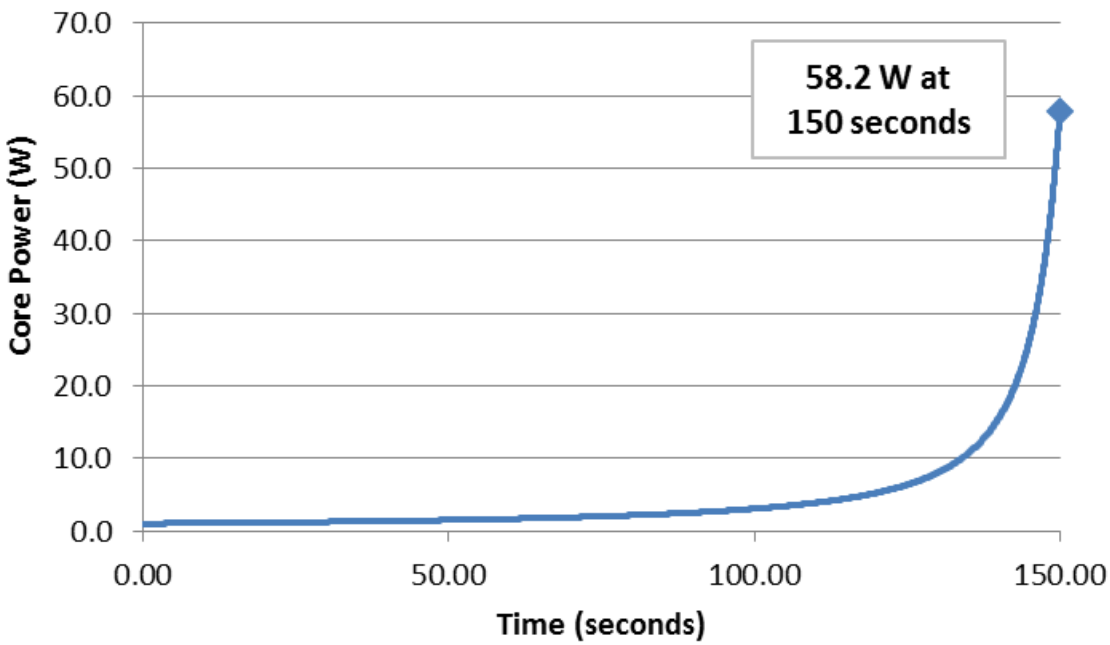

Figure 2.10. HEU Core Power During Simulation of Startup Accident.

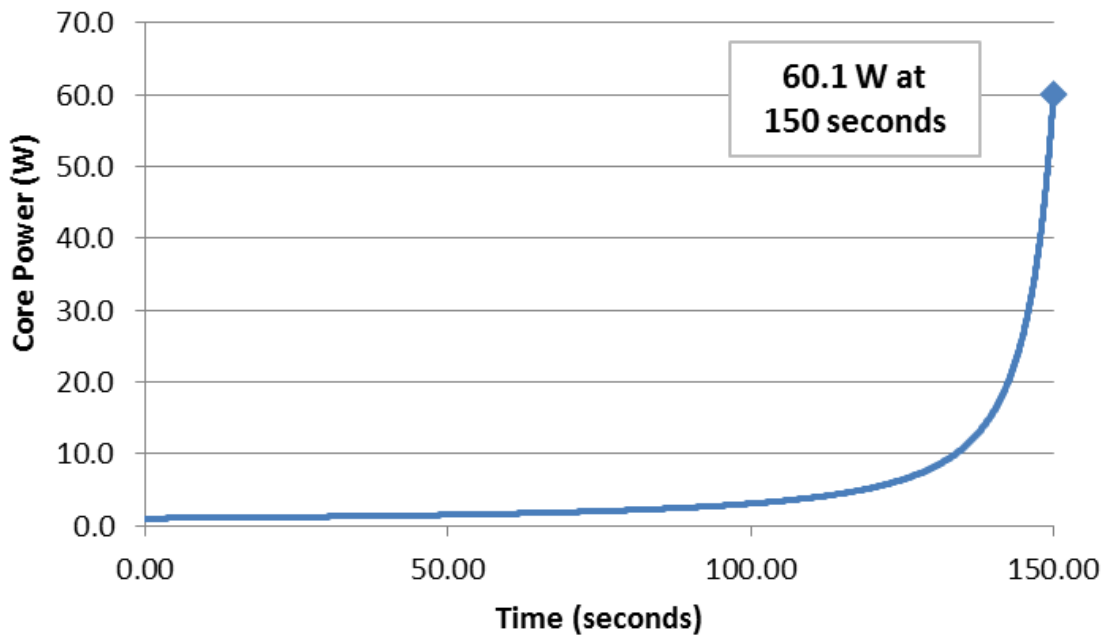

Figure 2.11. LEU Core Power During Simulation of Startup Accident.

2.4 Conclusions

The insertion of excess reactivity in the HEU-fueled and LEU-fueled MURR has been analyzed to assess the impact of a rapid step insertion of positive reactivity and the impact of a continuous control blade withdrawal accident.

The results of the first analysis showed that the MURR can withstand a positive reactivity step insertion of up to 0.006 Δk/k without core damage. This value is the MURR T.S. limit for the maximum allowed absolute reactivity worth of all experiments in the center flux trap. It also corresponds to the maximum allowed worth of each secured removable experiment and the sum of the reactivity worths of all unsecured experiments installed in the reactor. Smaller T.S. limits on the reactivity worths of individual unsecured experiments and individual moveable experiments also exist. The results demonstrate that the MURR can also withstand these smaller reactivity step insertions without core damage.

The consequences of a continuous blade withdrawal accident at the MURR will be a rod run-in or a reactor scram on either short period or high power and there will be no resulting fuel damage.

The results indicate that fuel conversion to a proposed U-10Mo monolithic fuel will result in no damage to fresh fuel plates for any of the reactivity insertion accidents postulated for MURR. In the Phase II analysis, the impact of fuel burnup, oxide layer growth, and coolant channel restriction due to oxide growth and fuel creep on the accident results will be assessed.

3.0 LOSS OF COOLANT AND LOSS OF FLOW ACCIDENTS

3.1 Background and Goals

"Chapter 13, Accident Analyses", of the University of Missouri Research Reactor (MURR) Safety Analysis Report (SAR) demonstrates for the HEU core that various facility design features, safety limits, limiting safety system settings (LSSSs), and limiting conditions for operation ensure that no credible accident can lead to unacceptable radiological consequences to people or the environment. In particular, Chapter 13 of the SAR demonstrates that for all credible loss-of-primary-coolant (LOCA) and loss-of primary-flow (LOFA) accidents unacceptable consequences to people and the environment are avoided. For the conversion of the MURR core from HEU fuel to LEU fuel it is necessary to provide an analogous demonstration for the LEU core that is to replace the HEU core and to demonstrate adequate safety margins for the LEU core. Also, the performance of the two cores must be compared using consistent modeling assumptions.

The HEU core accident analysis of the SAR was performed with the aid of the RELAP5 code [6]. The MURR RELAP5 model that was used for this analysis is described in considerable detail in "Appendix C, Thermal-Hydraulic Transient Analysis", of the MURR SAR. This substantial model explicitly represents all 25 coolant channels and all 24 fuel plates of the limiting fuel element and includes the primary coolant loop and the pool loop. The model is largely the result of collaboration between the MURR staff and a private consultant. Separate RELAP5 input files of some 8000 lines each were produced for each accident scenario.

The current effort is to be accomplished in two phases. The first phase, Phase I, which is documented by this report, is to obtain an initial comparison of the performance of the HEU and LEU cores during LOCA and LOFA events and to make an initial assessment of the performance of the MURR with the proposed LEU core with regard to these severe accidents. During this phase of the modeling a few improvements were made to the MURR RELAP5 model, as described below. Then an LEU element model was substituted for the HEU one. The power distributions for both elements were taken from recent neutron physics analysis [1].

The knowledge gained during Phase I will be used to provide an early indication of the performance of the LEU core during severe LOCAs and LOFAs and to guide model improvements, where needed, to be implemented in Phase II. In the neutron physics analysis [1], detailed power distributions were predicted for a set of 24 potentially limiting HEU core states and the analogous 24 LEU core states. For the current Phase I accident analysis only the highest heat flux HEU core and the highest heat flux LEU core, 1B1 and 5B1, respectively, were modeled. These are beginning-of-cycle cores with no xenon. The following features are in this HEU and LEU models because they contribute to a higher nuclear hot spot peaking factor. The MURR flux trap has no holder or samples and is filled with only water. Control blades C and D are at eight years of depletion and are positioned 1 inch higher than control blades A and B, per the Technical Specification limit. Control blades A and B are fresh. In each of these two cores the HEU element and the LEU element with the highest heat flux are explicitly represented in the RELAP5 model. These elements are element X7 of the 1B1 HEU core and element X6 of the 5B1 LEU CD35 core. In Phase II additional HEU and LEU cores may be considered, and the RELAP5 model may be modified to explicitly treat distinct elements.

3.2 Accidents to Be Considered

Chapter 13.1 of NUREG-1537 postulates nine events or categories for research reactors to consider. Among these nine are the loss of primary coolant accident (LOCA) and loss of primary coolant flow accident (LOFA). Figure 3.1 provides a simplified schematic view of the MURR primary coolant system

and indicates the flow path during normal operation. A portion of the cold-leg coolant leading to the reactor core is shown in blue. A portion of the hot-leg coolant exiting the reactor is shown in red. The primary vessel boundary is shown in green. The locations of the cold-leg core-inlet isolation valve 507B and the hot-leg core-outlet isolation valve 507A are indicated. A reactor scram occurs and these valves close automatically during depressurization accidents and are designed to limit the loss of coolant from the core in the event of a breach upstream of the 507B valve or downstream of the 507A valve. The portion of the primary coolant system that contains the core is located within the reactor pool. This limits the loss of coolant due to a primary loop breach that occurs within the pool boundary. Thus, the primary loop breaches of most concern are the ones that occur between the exterior of the pool wall and these isolation valves. Thus, the cold-leg LOCA and the hot-leg LOCA that are a result of a double-end pipe-break of one of the two 12-inch diameter sections of piping between the pool wall and the 507 A and 507B isolation valves were analyzed in the MURR SAR and are analyzed in this report.

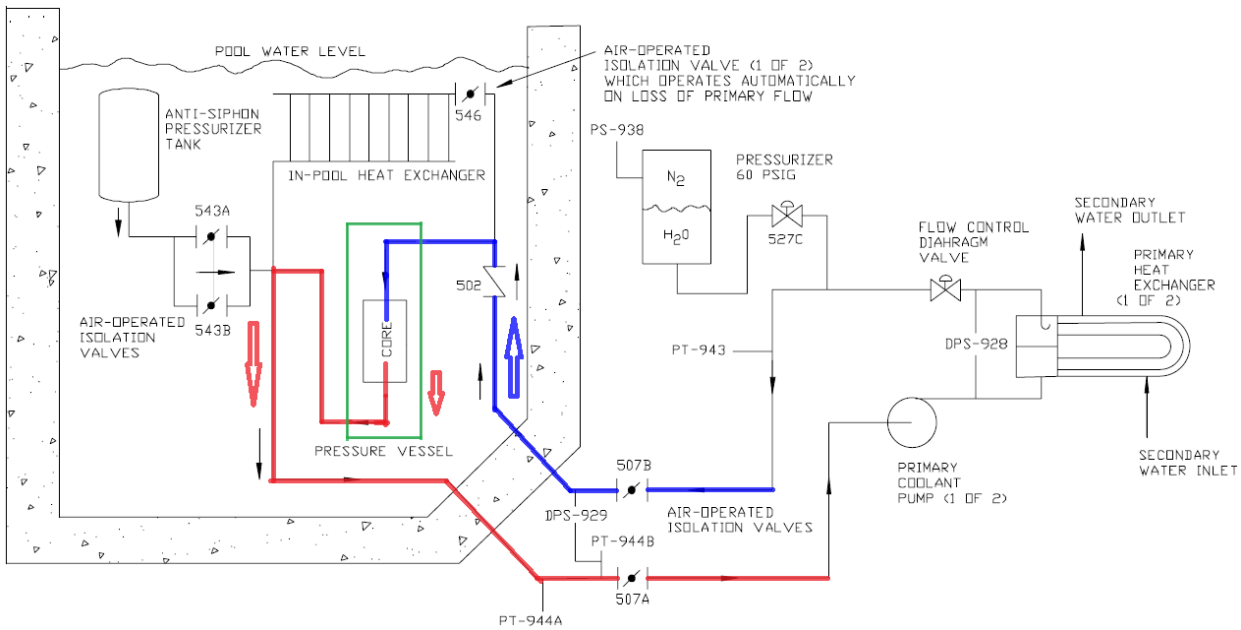

Figure 3.1. Simplified Schematic of MURR Primary System Loop (Normal Path).

The MURR SAR considered five possible anomalies as potential initiators of loss of primary flow accidents (LOFA). These are:

(a) Loss of facility electrical power (or coolant circulation pump power);
(b) Inadvertent closure of coolant loop isolation valve(s);
(c) Inadvertent loss of pressurizer pressure;
(d) Locked rotor in a coolant circulation pump; and
(e) Failure of a coolant circulation pump coupling.

The MURR SAR considered all five and concluded that the worst-case accident is (c). The SAR stated: "The LOF accident caused by a loss of pressure in the primary coolant system pressurizer can be initiated by anomalies such as a break in any of the piping penetrations near the top of the pressurizer, a failure of the pressurizer relief valve, or pressurizer nitrogen vent valve V545 failing in the open position." All of these scenarios result in loss of pressure in the pressurizer, which causes a primary loop depressurization through the 2-inch diameter line that connects the pressurizer to an 8-inch pipe in the primary loop, Figure 3.1. However, a more rapid depressurization of the primary loop after the 507A outlet valve and before

the 507B inlet valve would occur via a rupture of the diaphragm in either of the flow control diaphragm valves, valve 540A or B. As shown in Figure 3.1, this valve is upstream of where the 2-inch line from the pressurizer joins the 8-inch primary loop pipe. Moreover, this upset happened in the MURR plant in April 2008. Therefore, this LOFA accident will be studied in place of a rupture in the 2-inch line leading from the pressurizer to the 8-inch line. In the accident analysis it will be assumed that an 8-inch diameter breach, which is not a double-ended breach, occurs at the 540 valve. This piping is 8-inches in diameter instead of 12-inches because in the plant two parallel 8-inch pipes merge where they join the 12-inch piping that connects to the reactor. Each 8-inch piping run includes a primary pump, a heat exchanger, and a 540 throttle valve. In the model the two 8-inch paths are merged into a single equivalent path.

Thus, for Phase I, the following three depressurization accidents will be analyzed for both an HEU core and an LEU core:

1. Cold-leg LOCA – double-end 12-inch diameter break at the core side of the 507B cold-leg isolation valve.
2. Hot-leg LOCA – double-end 12-inch diameter break at the core side of the 507A hot-leg isolation valve.
3. LOFA – 8-inch diameter breach in the 8-inch cold-leg piping at the flow control diaphragm valve.

Because all of these accidents are initiated by a depressurization of the primary loop, the automatic actions taken by the plant protection system are the same in each instance. A reactor scram is promptly initiated, the primary pumps are tripped, the anti-siphon valves are opened, the two primary loop isolation valves (507A and 507B) are closed, the valves to the in-pool heat exchanger are opened, and the pressurizer isolation valve, 527C is closed. These actions rapidly reduce the reactor power to decay heat levels and tend to minimize the loss of coolant from the plant.

Figure 3.2 provides another copy of the simplified schematic view of the MURR primary coolant system, but with the coolant paths highlighted during a LOFA after the two primary loop isolation valves have fully closed and the in-pool heat exchanger isolation valves 546A and 546B have opened. In this situation natural circulation will cause a flow reversal in the core, resulting in upward flow through the core and downward flow through the in-pool heat exchanger. The hot coolant exiting the core is indicated in red and the cool flow exiting the in-pool heat exchanger is shown in blue. An additional important mode of heat transfer is directly from the primary coolant through the aluminum reactor pressure vessel walls to the pool coolant. There is a separate pumping system that maintains forced pool coolant flow through the flux trap inside the inner reactor pressure vessel and in the control blade channels on the outside of the outer pressure vessel wall. This forced flow is maintained throughout the transients that are under consideration.

The anti-siphon tank is designed to inject air into the top of the primary coolant inverted loop so that in the event of a break in the hot-leg piping beyond the pool wall, water will not be siphoned from the primary vessel and thereby cause the core to become uncovered. The 502 check valve on the primary inlet pipe riser, shown in Figure 3.2, serves the analogous role with regard to a break in the inlet piping outside of the pool wall. This check valve limits flow in the downward direction to only the primary coolant between the inlet side of the check valve and the 507B isolation valve.

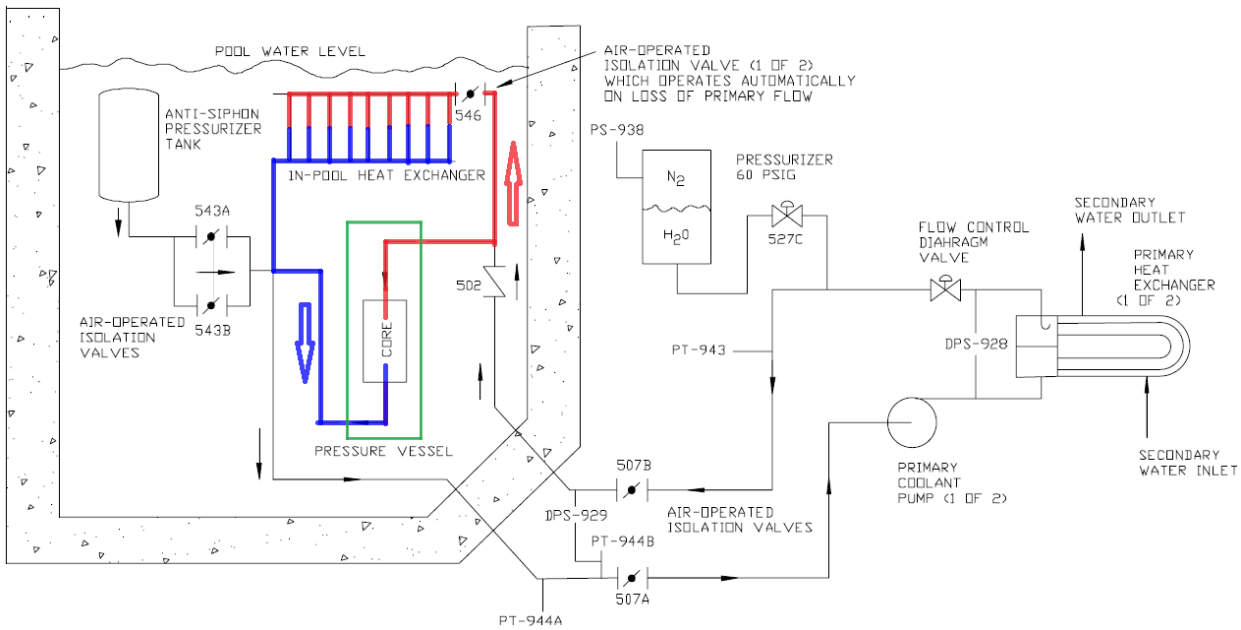

Figure 3.2. Simplified Schematic of MURR Primary System Loop (LOFA Upset Path).

Figure 3.3 provides another copy of the simplified schematic view of the MURR primary coolant system, but with the coolant paths highlighted during a hot-leg LOCA after the primary loop inlet isolation valve 507B has fully closed. However, this time there is stagnant cold water in the paths that are show in blue that are outside the vessel. Since the break is outside the pool wall and before isolation valve 507A, the anti-siphon air flow breaks any siphon of the outlet pipe from the anti-siphon connection to the 507A valve. Water can drain out through the break and air can enter through the break and fill the in-pool heat exchanger. The reactor inlet leg is filled with liquid up to the top of the vertical rise, as shown in blue. The outlet leg from the reactor vessel is full of liquid up to the top of the outlet vertical riser, as shown in blue. The flow path through the reactor is natural recirculation among the coolant channels of the core with upward flow in the hotter channels and downward flow in the cooler channels. This recirculation includes flow down the first and last channels, since they are cooled by the inner and outer vessel walls, and up flow through many of the hotter channels in between them. Thus, the red path at the top of the core is designed to show many hot upward-flow channels in the core. The path below the core is blue indicating this section of pipe is close to being in equilibrium with the pool coolant temperature. The upward hotter channels' flow results in the coolant above the core being hotter than the coolant below the core. The total upward flow must equal the total downward flow even if there may be more channels with upward flow than with downward flow, but the downward flow does not go too far past the coolant channel bottom outlet before reversing and going up in the hotter channels.

Figure 3.4 provides yet another copy of the simplified schematic view of the MURR primary coolant system, but with the coolant paths highlighted during a cold-leg LOCA after the one remaining primary loop outlet isolation valve, 507A, has fully closed. This is very similar to the hot-leg LOCA configuration of Figure 3.3. The only difference here is that part of the hot leg is filled with liquid, as shown in blue, because the hot leg is intact and the 507A isolation valve is closed. Before the 507A isolation valve has fully closed, the anti-siphon system has injected air into the inverted loop that occupies part of the outlet leg. Flow within the core where it exists is by recirculation among the channels, as in the hot- leg LOCA. The MURR primary system has a vent tank located a considerable distance from the

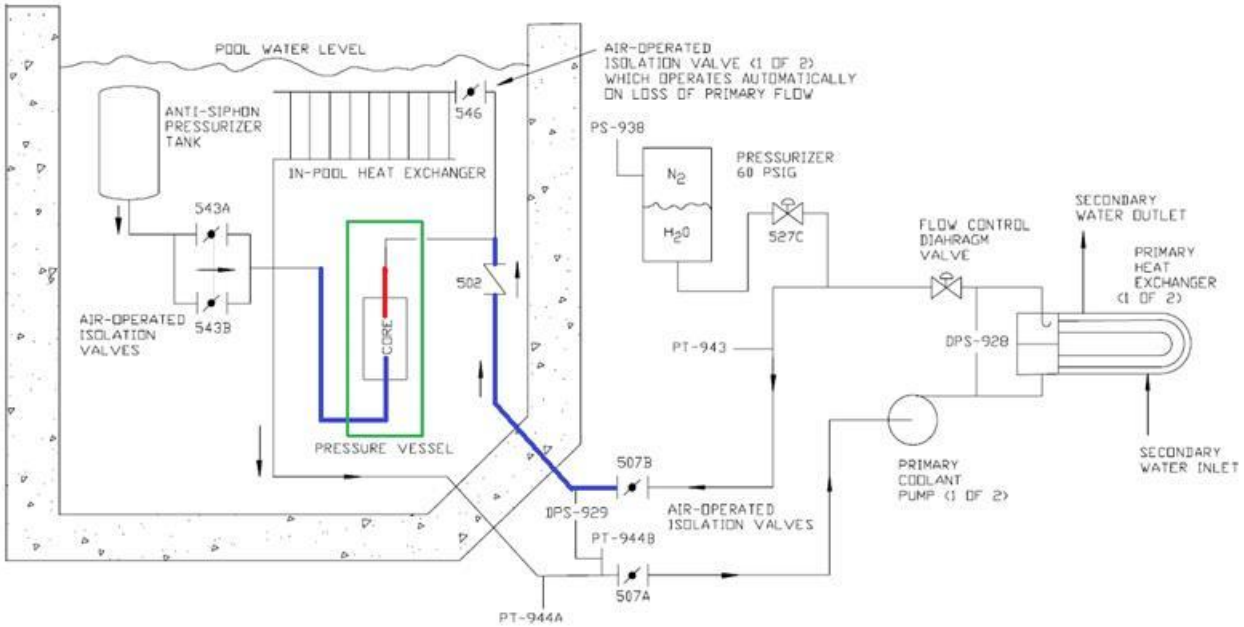

Figure 3.3. Simplified Schematic of MURR Primary System Loop (Hot-Leg LOCA Configuration).

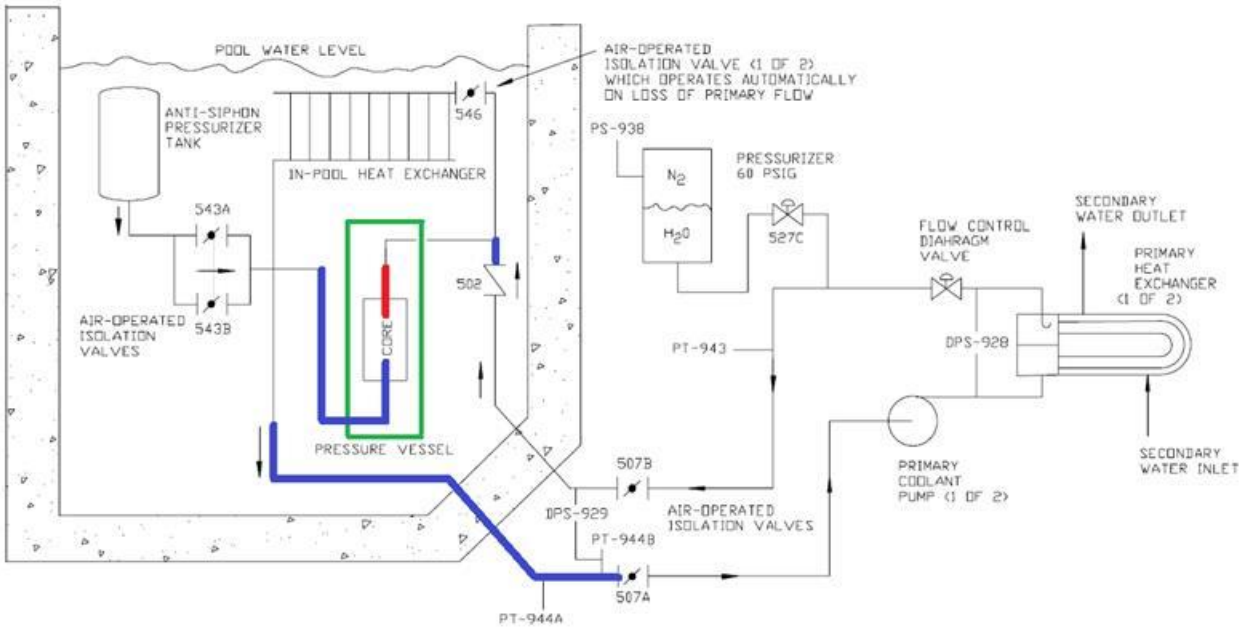

Figure 3.4. Simplified Schematic of MURR Primary System Loop (Cold-Leg LOCA Configuration).

reactor. A ½-inch tube connects the top of the in-pool heat exchanger to the vent tank, which is within the primary system pressure boundary. Small volumes of gases, such as air and vapor, can escape through this tube to the free surface of the vent tank. Water from the vent tank would flow downward through the same tube as air bubbles rise upward through the same tube. However, the amount of water lost in a LOCA is much greater than the small inventory of water in the vent tank so there is not enough water to fill the gas pocket in the in-pool heat exchanger during the cold-leg LOCA.

A comparison of the hot-leg and the cold-leg LOCAs should make it clear that they both depend on potential flow recirculation among the core channel and heat transfer through the aluminum pressure vessel walls to the flowing pool coolant loop for long-term heat removal. The major difference between the two transients is in the initial seconds. The break before the core inlet in the cold-leg LOCA tends to slow the core flow, while the break after the core outlet in the hot-leg LOCA tends to speed the flow, or at least maintain it. This is due to the cold-leg LOCA instantly removing the coolant pressure pushing the coolant up through the 502 check valve in the core, reversing the flow direction on the 502 valve inlet side and draining down out the pipe break at the 507B valve, which slows the core flow rate. The hot-leg LOCA instantly reduces the pressure at the 507A valve which maintains the core flow rate. During the first few seconds of the transient the LOFA can have core flow behavior that is in between the two LOCAs in that it is a milder version of the cold-leg LOCA.

3.3 Model

3.3.1 Model as Provided in the MURR SAR

The structure of the RELAP5 model used to represent the MURR reactor with its HEU core is described in considerable detail in “Appendix C, Thermal-Hydraulic Transient Analysis” of the MURR SAR. This model explicitly represents the core, the primary piping, the primary pumps, the primary heat exchangers, the pressurizer, the in-pool heat exchanger, the anti-siphon tank, the pool loop, and the plant protection system. However, as stated above, in the model the two parallel paths, each with its own primary pump, heat exchanger, and diaphragm valve, are merged into a single equivalent path with one heat exchanger, one pump, and one diaphragm valve. Also, the two parallel air-operated anti-siphon valves and the two parallel air-operated in-pool heat exchanger valves are each modeled as a single valve.

The potential for fuel damage is assessed by predicting the peak fuel plate centerline temperature. As indicated earlier, for the HEU core all 24 fuel plates and 25 coolant channels of the highest power element are explicitly modeled. Each fuel plate is divided into four axial nodes. The first and last node are each 7.75 inches long and the middle two nodes each are 5.0 inches long, for a total plate length of 25.5 inches. In each node the fuel meat and its two cladding layers, one on each side, are explicitly represented. Thus, in the analysis $4 \times 24 = 96$ fuel centerline temperatures are predicted as a function of time for each transient analyzed. In this model the geometry of the 0.75 inches of unfueled length at either end of the fuel plate is lumped in with the first and last nodes of the fuel plate and the power generated in the top and bottom nodes are each smeared over 7.75 inches. Also, all of the plate power is distributed among the four axial nodes. Thus, the model does not consider variations in power along the azimuthal direction of the curved fuel plates.

3.3.2 Recent Modifications to the MURR RELAP5 Model

3.3.2.1 RELAP5 Reactor Trip and Plant Protection System Model

The choice of HEU or LEU core does not affect the configuration of the plant protection system. A systematic review of the MURR plant protection system as it affects the RELAP5 models under consideration was performed. The six trips of concern are as follows:

- Trip 1 – core outlet pressure ≤ 40.7 psia
- Trips 2 and 3 – primary flow ≤ limiting safety system setting (LSSS) flow (The LSSS flow for the HEU core is 3200 gpm of water at 155°F. The LSSS flow for the LEU core is 3300 gpm of water at 145 °F density.)
- Trip 4 –pressure at the junction of the two primary heat exchanger loops ≤ 72.2 psia
- Trip 5 –pressure drop between valves 507B and 507A ≤ 24.8 psia
- Trip 7 – core outlet isolation valve 507A starts to close
- Trip 8 – core inlet isolation valve 507B starts to close

The trip numbers correspond to those used in the operation of the MURR facility. More specific details, including delay times, are provided for these six trips in Figures 3.5 through 3.10, respectively. A concerted effort was undertaken to obtain accurate upper limits for delay times. In these six figures the value to the left of the "|" symbol is the additional delay time prior to taking the action to the right of the "|". For example, in trip 1 when the core pressure drop drops to 40.7 psia, there is a 0.3 s delay to de-energize the relays 2K13 and 2K28. There is a 0.2 s delay after the opening of theses relays, before a scram signal is sent. Then after a 0.1 s delay the rods start to drop. All of the actions listed in the eight trips are the start of the action. The 507A and 507B isolation valves, for example, require a few seconds before they start closing and take a few additional seconds to go from fully open to fully closed.

Trip 6 is based on the liquid level in the pressurizer, which is not included in the above list because the liquid level in the pressurizer is not part of the RELAP5 model. This trip closes valve 527C, Figure 3.1, which isolates the pressurizer from the main steam line. This valve is also closed by trips 7 and 8. The function of this valve in the plant is to preserve the water inventory in the pressurizer. In both the MURR SAR RELAP5 model and in the current models the timing of the closing of this valve is important because the pressurizer is treated as a constant pressure source rather than a volume that loses pressure as the transient progresses. Thus, if this valve is not closed in a timely manner, inappropriately higher pressures are predicted for the core, which, in turn, affects the temperatures predicted in the core. Because the decreasing pressurizer level and pressure are not modeled, in the current RELAP5 model, a limiting assumption is made, which is to close this valve at the initiation of any primary system depressurization transient. In the past MURR RELAP5 modeling, the 527C valve was closed, but typically after the peak temperatures were predicted rather than at the initiation of the depressurization transient. A possible consequence of higher core pressures is less boiling. Maintaining the core pressure can either raise or lower the fuel temperatures. This is because, as Figure 3.11 shows, raising the pressure from atmospheric pressure (14.7 psia) to 25 psia, for example, raises the saturation temperature of the coolant by 28 °F to 240 °F. The fuel temperature tends to follow the adjacent coolant temperature. However, a 28 °F increase in fuel temperature is a relatively minor matter when considering severe accidents. A much bigger concern is that the increased boiling that accompanies a decrease in pressure can lead to heat transfer modes beyond subcooled nucleate boiling that can produce much greater increases in fuel temperature.

In the currentRELAP5 models for the HEU and LEU cores all of the trips on the above bullet list are explicitly represented in the model.

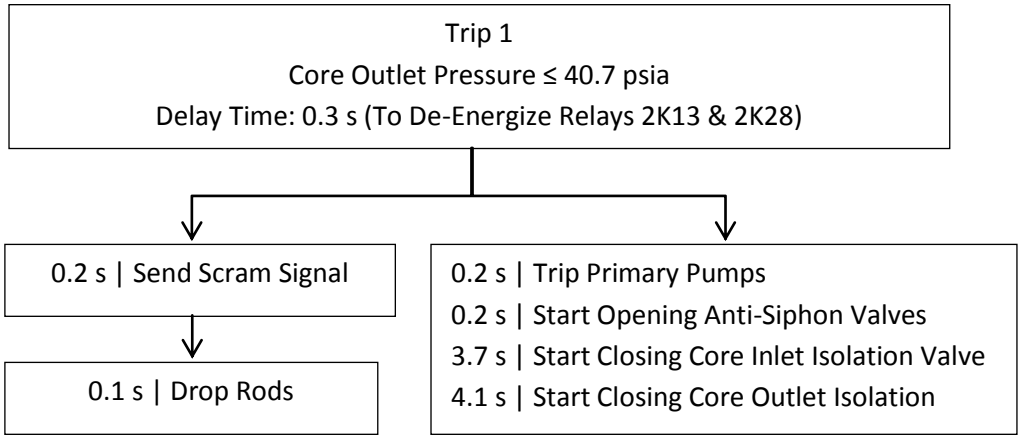

Figure 3.5. Trip 1: Core Outlet Pressure.

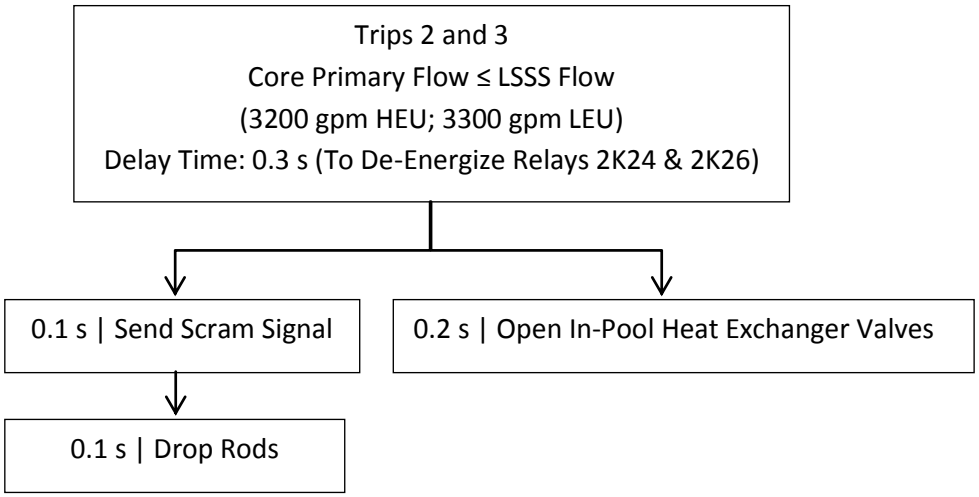

Figure 3.6. Trips 2 and 3: Primary Flow.

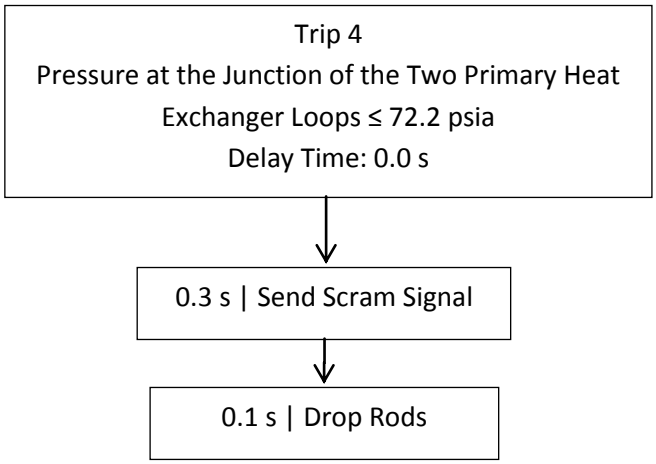

Figure 3.7. Trip 4: Core Inlet Pressure.

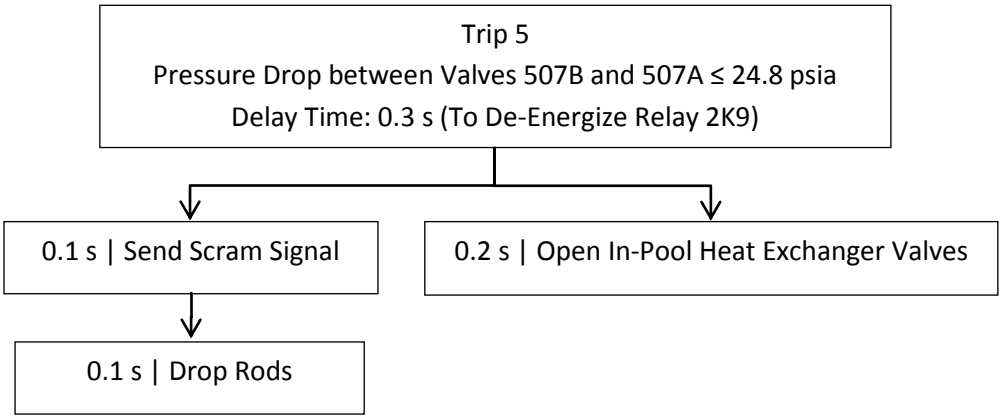

Figure 3.8. Trip 5: Core Pressure Drop.

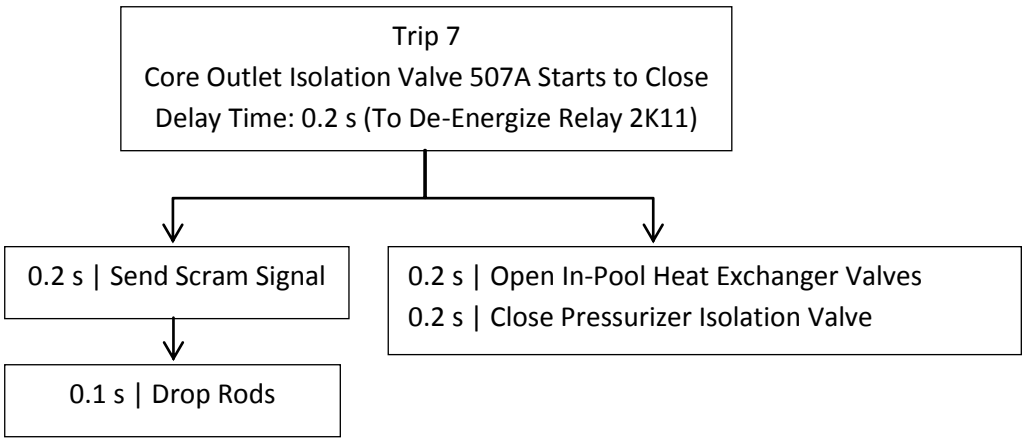

Figure 3.9. Trip 7: Core Outlet Isolation Valve Starts to Close.

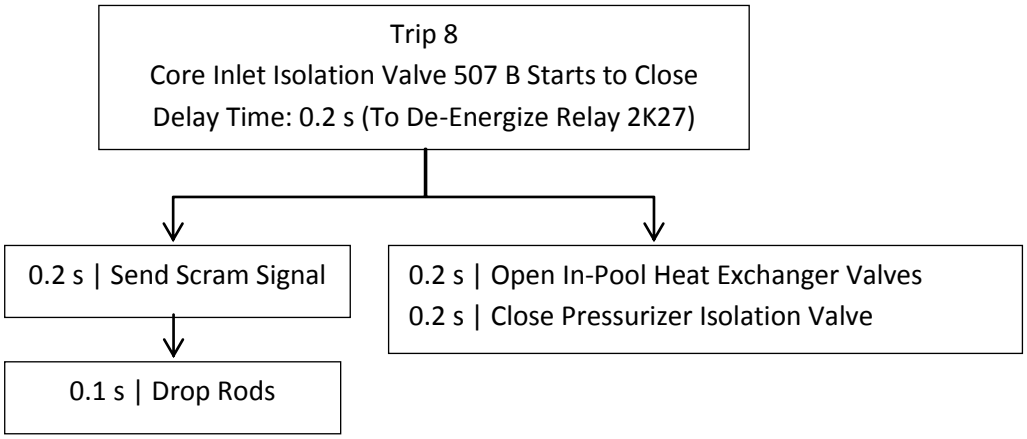

Figure 3.10. Trip 8: Core Inlet Isolation Valve Starts to Close.

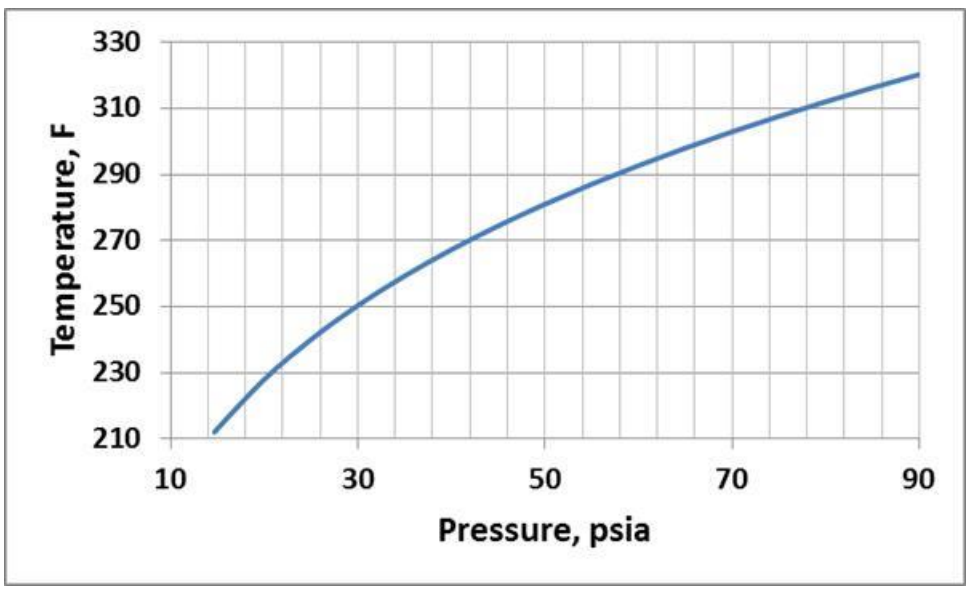

Figure 3.11. Saturation Temperature of Water.

3.3.2.2 Improved Core Channel Hydraulic Diameters, Laminar-Flow Friction Shape Factors, and Relative Roughness

The original MURR RELAP5 models used RELAP5 default values for both the hydraulic diameters of the core channels and the laminar-flow friction shape factors. The RELAP5 default is that the hydraulic diameter is the diameter of a circular duct of the same flow area. In thin rectangular channels of very small aspect ratio the hydraulic diameter is approximately twice the channel thickness, which can be far from this default value. Therefore, for both the HEU and the LEU core, new hydraulic diameters were explicitly calculated and used in the models, based on four times the flow area divided by the wetted perimeter of the channel. The original model made all of the hydraulic diameters too large, with the effect getting more pronounced with increasing channel flow area in going from the inner vessel wall to the outer. Making the hydraulic diameter of a particular channel larger reduces the hydraulic resistance of

that channel and thereby incorrectly increases its velocity. At the initial steady-state condition, where the total flow is fixed, the net effect is to redistribute flow away from the smaller-area channels near the inner vessel wall and toward the larger-area channels near the outer vessel wall.

For laminar flow the Moody friction factor, f, is given by f = C/Re, where Re is Reynolds number and C is a constant. The RELAP5 default value for C is 64 because it is based on the assumption that the duct is circular. For rectangular ducts, Kakac *et al*. propose a reasonably close approximation for C as 4 times the value of $C_{Fanning}$ given by equation 3.158 on page 3.46 of Reference 12:

$$C_{Fanning} = 24 \times (1 - 1.3553\, a + 1.9467\, a^2 - 1.7012\, a^3 + 0.9564\, a^4 - 0.2537\, a^5),$$

where a is the duct aspect ratio. The factor of 4 is needed for RELAP5 application because the equation in the reference is for the Fanning friction factor, which is $1/4^{th}$ of the Moody friction factor. The RELAP5 code assumes that f for laminar flow is given by 64/(Re Φs), where Φs is an input shape value, whose default value is 1.0. Thus, Φs = 64/C. As Tables A-1 and A-2 of Appendix A show, Φs varies from channel to channel of the MURR HEU and LEU fuel designs, but is always close to 0.7.

The maximum allowed absolute roughness for the MURR fuel plates, based on existing MURR drawings, is 63×10^{-6} inches, or 5.25×10^{-6} feet. The value used in the original model is 10×10^{-6} feet. Although this value is about twice as large as it should be, the effect of the core flows, and more importantly, on the peak fuel temperature, should be very small. In the current RELAP5 models of the HEU and LEU cores, the absolute roughness is set to 63×10^{-6} inches.

All of the flow areas, hydraulic diameters, and laminar flow shape factors were calculated for all channels in the fresh HEU and LEU elements and are provided in Tables A-1 and A-2 of Appendix A. These are the values that were used in the current modeling. The flow area of each channel in the MURR HEU or LEU core is calculated as the product of the channel arc length and the channel thickness. The channel arc length is calculated at the average of the two bounding radii and is the 45° arc length diminished by 0.340 inches. This 0.340 inches accounts for the arc length occupied by the two 0.150-inch thick side plates and 0.040 inches between the side plates of adjacent elements.

3.3.2.3 Core Heat Transfer Areas and Nodal Structure

The nodal structure of the fuel plates with four axial nodes per plate that was used in the original MURR RELAP5 model was used in the current analysis. RELAP5 only permits curved heat transfer structures for closed, 360°, annuli and cylinders. Therefore, the curve plates of the MURR plate are modeled as flat plates with the plate width dimensions based on the values at the average of the inner and outer radii. For both cores the values of heated perimeter and heat transfer area were calculated for all of the nodes in the HEU and LEU cores and are tabulated in Tables A.3 and A.4 of Appendix A. In the calculation of the heat transfer areas, the fuel meat arc length is the 45° arc length at the average radius of the plate reduced by 0.492 inches. Each vertical edge of a fuel plate is inserted into a side plate groove. If the fuel plate bottomed in the groove the fuel meat would start 0.070 inched from the edge of the channel and the 0.492-inch value would be 0.340 + 2 × 0.070 = 0.480 inches. However, to allow for manufacturing assembly clearances, the fuel plate arc length is made 0.012 inches shorter than the arc length between the bottoms of the side-plate grooves.

3.3.2.4 Secondary Sides Were Added to Primary and Pool Heat Exchangers

In the original MURR RELAP5 model the flows on the secondary sides of the primary and pool heat exchangers were not modeled. Instead the heat removal rate from each of these two heat exchangers was specified as functions of time to obtain the desire coolant temperatures. These functions had to be

properly set at the initial steady-state conditions so the heat removal rate from each loop was correct. Each function reduced the heat removal rate to relatively very low values over the first 5 s of the transient so that excessive heat removal would not follow the scram. The desired temperature of the coolant in the cold leg of each loop during the initial steady-state condition was approximately achieved via a bounding node in each loop where temperature and pressure were set. In the RELAP5 code this node is referred to as a "time-dependent volume". Although this approach is quite adequate, a different method that was fairly easy to implement is to include a secondary side to the heat exchangers. For both heat exchangers a counter-flow heat exchanger was modeled in which the initial steady-state flow on the secondary side was approximately equal to that on the primary side. The secondary flows were reduced to relatively very low values over the first 5 seconds of the transient. A trial-and-error method was used to obtain the inlet temperatures to the secondary sides of the heat exchangers that produced the desired cold-leg temperatures for the primary and pool loops, which in the RELAP5 models were observed at the first primary-side node after the heat exchanger. RELAP5 was executed multiple times to calibrate the steady-state solution by adjusting the secondary side inlet temperatures (nodes 910 and 751 of the heat exchangers) until the desired cold-leg loop temperatures were obtained (node 1 of pipe 115 and node 5 of pipe 700).

3.3.2.5 Fuel Thermal Properties

All of the thermal property values discussed in this section, including the HEU values in the original MURR RELAP5 model and the values applied in the current HEU and LEU models, are tabulated in Table A.5 of Appendix A.

The value of thermal conductivity for the fresh HEU fuel meat can be obtained from Reference 13. In Table 4 on page 22 of this reference, the volume-% of UAlx of 35.4 was added to the percent porosity of 6 to obtain a total value of 41.4. Then in Figure 8 on page 27 of the reference, at 41.4 Volume Percent (fuel + voids), the open square symbols indicate that the thermal conductivity is about 40 to 45 W/m-C (0.00642 to 0.00722 Btu/s-ft-F). Therefore, 0.00642 Btu/s-ft-F (40 W/m-C) was used for fresh HEU fuel in the core steady-state analysis of Reference 5. This value is much smaller than the approximately 0.012 Btu/s-ft-F (75 W/m-C) values in the original MURR RELAP5 model. Hence, for the current analysis, the value was changed to 0.00642 Btu/s-ft-F (40 W/m-C). A check of the values of the fuel heat capacity in the original model was made, and the values are deemed acceptable for preliminary analysis.

For the LEU fuel, values of thermal conductivity and the product of density and heat capacity for both zirconium and for the U-10Mo fuel foil were needed for the LEU core model. Zirconium thermal properties were obtained from Fink and Liebowitz [14]. Equation 8 of this paper is $k = 8.8527 + 7.0820e{-3}\ T + 2.5329e{-6}\ T^2 + 2.9918e3\ /\ T$, where k is thermal conductivity in W/m-C and T is temperature in K. For temperatures from room temperature to 866 °C, equation 2 of this paper provides $C_p = 24.1618 + 8.75582e{-3}\ T - 69942\ /\ T^2$, where C_p is heat capacity in J/mol-C and T is temperature in K. Near equation 4 of this reference, which provides density as a function of temperature, the density at room temperature is given as 6.57 g/m^3. This appears to be a misprint and was taken be 6.57 g/cm^3. Since the atomic weight (or mass) of zirconium is 91.224, each mole weighs 91.224 grams. The conductivity function for zirconium has a minimum of 18.954 W/m-C at 277.4 °C (=531.3 °F) and behaves monotonically either side of this minimum over the range of interest.

Reference 8 provides the thermal conductivity, density, and heat capacity of U-10Mo Alloy. Page 2, equation 1, provides that $C_p = (0.137 \pm 3.31\times10^{-3}) + (5.12\times10^{-5} \pm 1.41\times10^{-5})\ T + (1.99\times10^{-8} \pm 1.29\times10^{-8})\ T^2$, where C_p is the heat capacity in J/g-C and T is fuel temperature and is between 100 and 1000 °C. The density, ρ, is given on page 5, equation 4, as $\rho = 17.15 - (8.63 \times 10^{-4} \pm 2.77 \times 10^{-5})\ (T + 20)$, where ρ is in g/cm^3 and T is temperature between 20 and 700 °C). The thermal conductivity, k, is given on page 7, equation 5, as $k = (10.2 \pm 0.688) + (3.51\times10^{-2} \pm 1.61\times10^{-3})\ T$, where k is in W/m-°C and T is temperature

between 20 and 800 °C. For the current analysis the nominal values were used and density was evaluated at room temperature, 68 °F (20 °C), and is treated as a constant.

3.3.2.6 LEU and HEU Core Models

Figure C.4 of Appendix C of the MURR SAR provides a nodal diagram of the HEU element with RELAP5 node numbers for the 24 fuel plates and 25 coolant channels. Since the LEU fuel element has one less fuel plate and one less coolant channel, for the LEU core model the fuel plate and the coolant channel that are closest to the outer vessel wall were deleted from the model. In Figure C.4 these are fuel plate nodes 624, 649, 674, and 699 and the four nodes of coolant channel 526. The nodes of the inner surface of the outer vessel wall that were connected to the four nodes of coolant channel 526, which do not exist in the LEU fuel element, were connected to the four coolant nodes of the new last coolant channel, channel 525.

The fuel plate, clad, fuel meat, and coolant channel thickness for all 23 plates and 24 coolant channels of the LEU core CD35 are tabulated in Table 1.1 of Reference 1. The clad thicknesses given in the table include the 0.001 inches of zirconium that is between the aluminum layer of clad and the fuel meat. For example, plate 1 is shown as having 17.5 mils (0.0175 inches) of clad. This corresponds to a 0.001-inch (1-mil) thickness of zirconium and a 0.0165-inch layer of aluminum clad on each side of the fuel meat.

Since in the RELAP5 model each HEU clad thickness was subdivided into three layers, adding the zirconium layer to the LEU model was relatively easy. For the LEU fuel plates, the layer of aluminum closest to the fuel foil was converted to zirconium and made 0.001 inches thick. The thicknesses of all of the aluminum and fuel foil layers were adjusted to correspond to the LEU CD35 values. All of the core coolant channel parameters, including flow area and hydraulic diameter, were also adjusted to correspond to those for the LEU CD35 core.

Table 3.1 summarizes the values of key reactor and pool parameters that were used in the MURR SAR analysis, the current HEU core analysis, and the current LEU core analysis and compares these values to those for normal operating conditions.

Table 3.1. Key Reactor and Pool Parameters.

Parameter	Normal Condition		HEU MURR SAR	HEU Current Analysis	LEU Current Analysis
	HEU	LEU			
Reactor Power, MW	10	12	11	11.04[1]	13.07[1]
Coolant Inlet Temperature, °F (°C)	120 (49)		155 (68)[2]		145 (63)[2]
Core Inlet Flow Rate, gpm (lpm)	3,800 (14,385)		3,800 (14,385)		
Pressurizer Pressure, psig (kPa)[3]	62 - 66 (427 - 455)		60 (414)[4]	67 (462)[4]	
Pool Temperature, °F (°C)	100		120[5]		
Anti-Siphon Pressure, psig (kPa)[3]	36 (248)		26 (179)		

[1]8 times the power of the element chosen for analysis.
[2]LSSS value.
[3]Pressure above atmospheric pressure of 14.7 psia (101.4 kPa).
[4]Pressurizer pressure in HEU model and SAR Table 13-1 are different. Basis and effect of the difference will be examined in Phase II.
[5]Technical Specification upper limit on pool coolant temperature.

The highest heat flux in the LEU CD35 core 5B1 is in plate 23 (outer plate) of element 6. The power distribution of element 6 is used in the RELAP5 modeling of the LEU core. This element produces 0.1361 of the total power that is produced by all eight elements. In effect, eight copies of this element were put in the RELAP5 model. This was accomplished with one element that has eight times the power and eight times the flow and heat transfer areas of a single element. 8 × 0.1361 = 1.089. The total power produced by the reactor in the model is 12 MW × 1.089 = 13.07 MW. However, as indicated on page 38 of Reference 5, 3.6% of the reactor power is deposited outside of the primary system. Therefore, in the RELAP5 model 3.6% of the 13.07 MW is allocated to the pool water, beryllium, and graphite reflectors and the other 96.4%, or 12.60 MW was assigned to the fuel element that represents the LEU CD35 core.

An analogous approach was used for the HEU core. The highest heat flux in HEU core 1B1 is in the first plate (plate 1) of element 7. The power distribution of this element was used in the RELAP5 modeling. This element produces 0.1380 of the total power that is produced by all eight elements. 8 × 0.1380 = 1.104. The total power produced by the reactor in the model is 10 MW × 1.104 = 11.04 MW. However, as indicated on page 38 of Reference 5, 6.0% of the reactor power is deposited outside of the primary system. Therefore, in the RELAP5 model 6.0% of the 11.04 MW is allocated to the pool water, beryllium, and graphite reflectors and the other 94.0%, or 10.38 MW was assigned to the fuel element that represents the HEU core.

The RELAP5 analysis of the HEU core in the MURR SAR assumed initial steady-state conditions of a total reactor power of 11.0 MW, a steady-state core flow rate of 3800 gpm, and a core inlet temperature of 155 °F, which are essentially identical to those that are used in the current analysis. Both analyses also assumed that the pool loop inlet temperature is 120 °F and that the initial air pressure in the anti-siphon tanks is 40.7 psia. The LEU analysis uses the same values for these parameters except that the total reactor power is about 2 MW higher and the core inlet coolant temperature is 145 °F.

Table C-3 of the MURR SAR provides the relative reactor power level as a function of time post trip, assuming 120 days full-power operation. The same power history and relative power level as a function of time was used in the current analysis.

3.3.2.7 Unified Models

The original MURR RELAP5 used a separate complete input file of approximately 8000 lines for each transient analysis. In each of these files the steady-state solution was obtained via a 500-s pseudo transient, which was immediately followed by the transient itself. The file contained the entire model and the added volumes and valves needed to simulate the particular rupture that initiated the transient.

Modeling of a break in a pipe is simulated by attaching an extra volume to the pipe where the break is to occur. This volume, which in RELAP5 is called a “time-dependent volume”, is at atmospheric pressure. A closed valve between this volume and the pipe represents an intact configuration. The break is simulated by suddenly opening the valve to initiate the transient. A LOCA is simulated by a double-end break, which requires two added valves and time-dependent volumes.

In the current modeling six added volumes and valves are employed, two near the cold-leg inlet to the core, two near the hot-leg outlet from the core, one near the 540 diaphragm valve, and one along the 2-inch pressurizer line. As described in Section 3.3.2.1, the revised plant protection system model includes all of the trips that are needed to model all of the transients to be studied.

As a further simplification, a 3000-s pseudo-transient was executed with none of the valves opened. This provided a steady-state solution that was used for all transients of the same core. The steady-state solutions were calibrated by adjustments in the inlet temperatures on the secondary sides of the primary

and pool heat exchangers to obtain the desired values of primary and pool loop inlet temperatures. Each transient was executed from a separate RELAP5 restart file that used a copy of a common (HEU or LEU) steady-state solution output file as the initial condition. A typical restart input file is only about 40 lines long, including comment lines. This file contains the delay times for the opening of the valves that simulate the pipe ruptures. The valves that represent active breaks were given delay times of 0. Those that were not to open during the particular transient were given delay times much longer than the transient simulation time. Each transient solution, which is a continuation of the 3000-s pseudo-transient steady-state solution, starts with 100 s of null transient before the accident occurs. This is to guarantee and demonstrate that the accident simulation is starting from a steady-state condition.

After a unified model was developed for the HEU core, it was used to develop a unified model for the LEU CD35 core. An important feature of the RELAP5 code is that the statements in the model input start with statement numbers and whenever a statement number is repeated it supersedes the earlier version of the statement in the file. Therefore, many of the statements that were needed to produce the current model were added to the end of the original MURR RELAP5 model. This makes changes to the model easier to track. The SNAP code [15] was used extensively in understanding and modifying the RELAP5 model. The SNAP code provides a visual nodal diagram of the RELAP5 model and has menus that allow the values of the parameters used in the model to be easily found and changed.

All of the RELAP5 results presented in this report were generated with RELAP5-3D, Version 4.0.3ie [16], which was provided by the INL code authors in executable form to run on a Windows PC. The code was executed in batch mode from a PC command window on a PC with a Windows 7 operating system.

3.4 Results

For both the HEU core and the LEU core, each of the three transients were executed for 2500 s. Figures 3.12 and 3.13 show the initial fuel centerline temperature distribution of each of the four axial nodes for all of the fuel plates in the core element of the RELAP5 model for the HEU and LEU cores, respectively. For each core the third node from the top has the highest temperatures in each plate, the top node has the lowest, and the second node from the top has the second lowest. In the HEU core the highest temperature occurs in plate 1, which is the plate closest to the flux trap. In the LEU core the highest temperature occurs in plate 23, which is the plate closest to the outer vessel wall.

The fuel centerline temperature history of all four nodes of all 24 fuel plates in the HEU model and all 23 plates in the LEU model were recorded for each 2500-s transient simulation. The maximum temperature of each node was determined for each of the three upsets simulated with RELAP5. For the HEU core the highest fuel centerline temperature occurred in node 3 of plate 2 in the cold-leg LOCA and in node 3 of plate 1 in the other two transients. For LEU core the highest fuel centerline temperature occurred in node 3 of plate 23 in all three transients. The fuel centerline temperature histories for these locations in the HEU and LEU cores are provided in Figures 3.14 and 3.15, respectively, for the first 4 s of each transient. In every case the peak fuel temperature occurs within the first second of the transient. The reason for this is that the scram, the time at which the rods start to drop, always occurs at about 0.41 s. In every case the peak is essentially coincident with the scram except for the cold-leg LOCA in the HEU core, where the peak occurs at 0.61 s. For both cores, Table 3.2 lists the peak fuel centerline temperatures for these nodes during steady-state and all three transients.

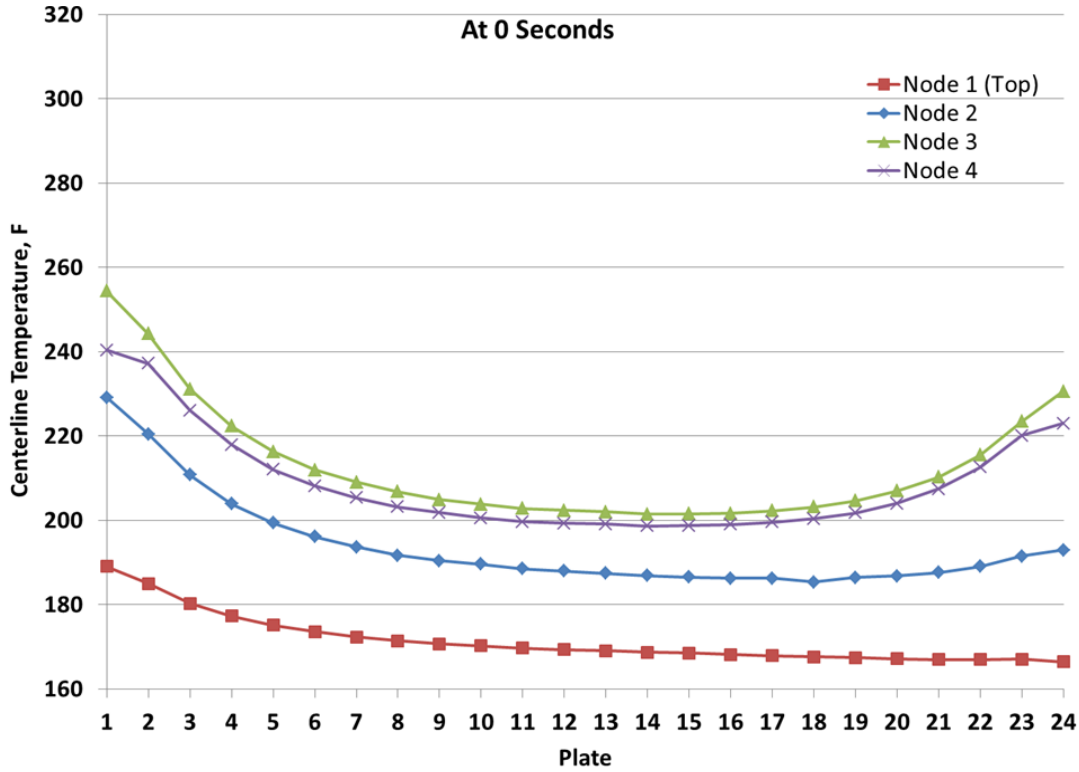

Figure 3.12. HEU Initial Fuel Centerline Temperatures.

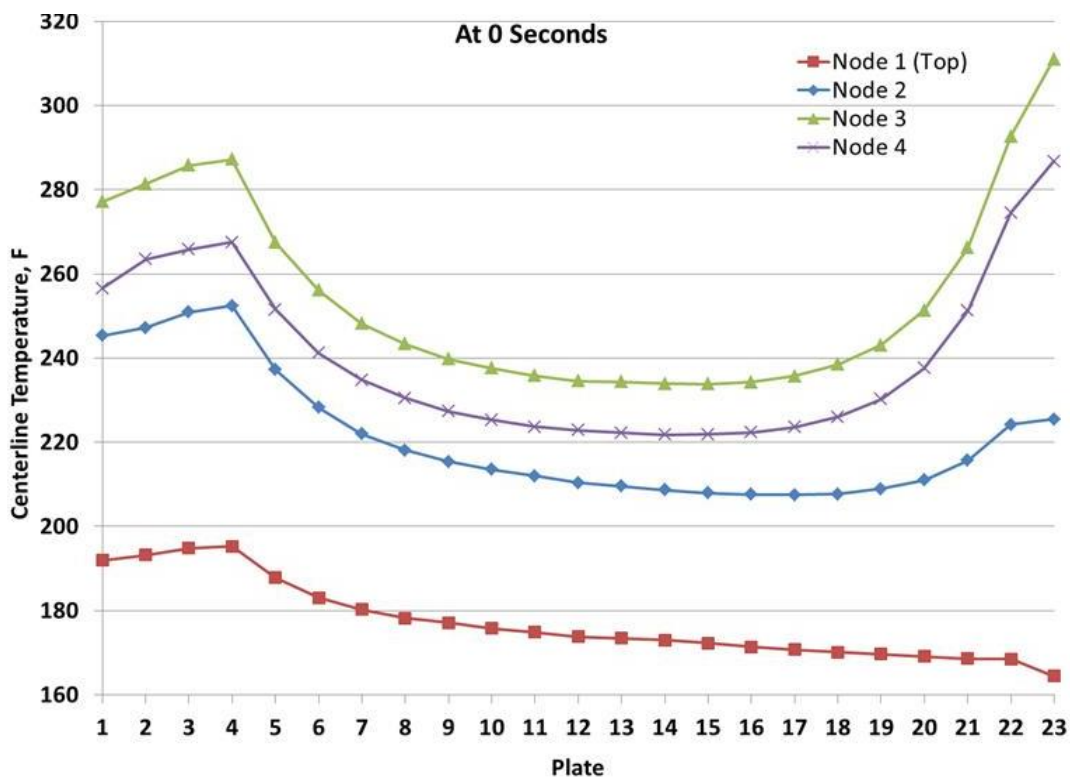

Figure 3.13. LEU Initial Fuel Centerline Temperatures.

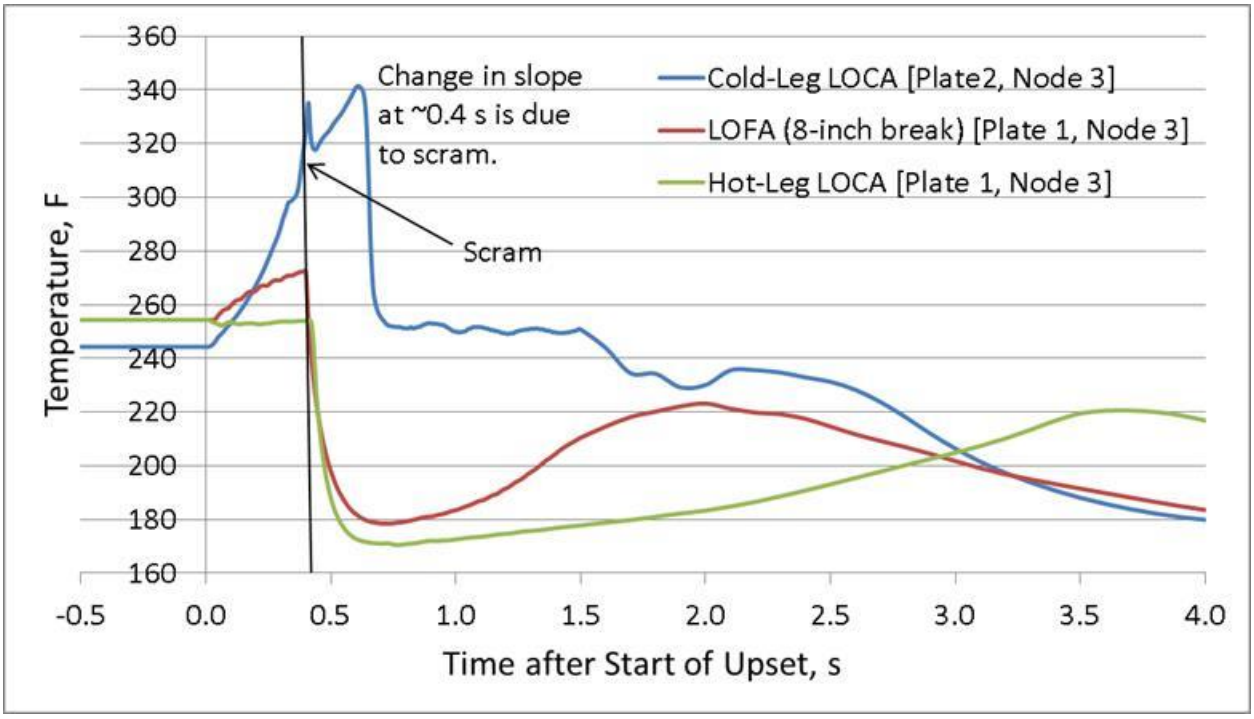

Figure 3.14. HEU Fuel Centerline Temperature History of Hottest Node.

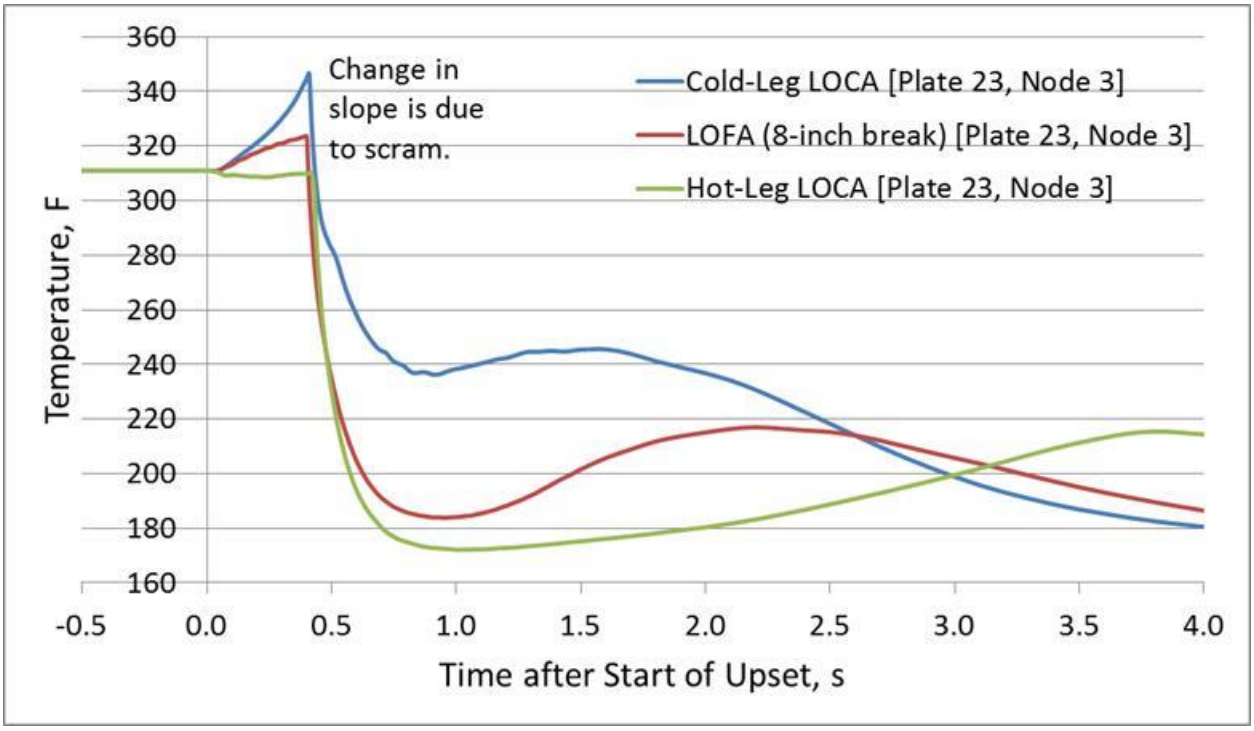

Figure 3.15. LEU Fuel Centerline Temperature History of Hottest Node.

Table 3.2. Fuel Centerline Temperatures for the Fuel Node of the Peak.

	Peak Temperature					
	Transient Value, ^{o}F	Time, s	Plate	Node	Steady-State Value, ^{o}F	Rise above Steady-State Value, ^{o}F
Current Model						
LEU						
Cold-leg LOCA	**346.5**	0.41	23	3	311.0	35.5
Large-break LOFA	323.5	0.40	23	3	311.0	12.5
Hot-leg LOCA	311.0	0.00	23	3	311.0	0.0
HEU						
Cold-leg LOCA	**341.5**	0.61	2	3	244.3	97.2
Large-break LOFA	272.6	0.40	1	3	254.4	18.3
Hot-leg LOCA	254.4	0.00	1	3	254.4	0.0
MURR SAR Model						
HEU						
Cold-leg LOCA	311.7	0.5	3	4	243.6	68.1
Small-break LOFA	280.3	0.3	1	3	272.1	8.2
Hot-leg LOCA	281.2	0.2	1	3	272.1	9.1

For each core the highest temperature occurs in the cold-leg LOCA and the lowest occurs in the hot-leg LOCA. This is due to the transient behavior of the flow in the core, as shown in Figures 3.16 and 3.17 for the HEU and LEU cores, respectively. Velocity is estimated using the mass flow at the junction between the second and third axial coolant nodes of each channel and the initial steady-state cold-leg density. As these figures show, the flow is drawn toward the break. Thus, the break in the cold leg just after the 507B isolation valve immediately attempts to reverse the flow in the inlet pipe. This causes the 502 check valve to close and stop the flow in the inlet pipe. This severely retards the flow in the core and causes it to approach zero even before the primary pump trip, which occurs between 0.50 and 0.53 s in all six cases. Similarly a break in the hot leg near the core exit initially tends to accelerate or at least allow the core flow rate to be maintained near to its initial steady-state flow until the pump trip occurs. The break in the cold leg that initiates the LOFA affects a core flow rate change during the first few seconds that is in between the cold-leg and hot-leg LOCAs. This break is further from the core inlet than in the cold-leg LOCA and is a less severe break in that it is not double ended.

In the HEU cold-leg LOCA the peak temperature occurs about 0.2 s after the scram rather than essentially at the scram, as occurs in all of the other five cases presented. This behavior may seem anomalous because the power decreases dramatically with the scram and the flow is near zero before the scram is reached. However, the other important parameter is the heat transfer from the fuel plate. As the top panel of Figure 3.18 shows, the void fraction is nearly 1.0 on both the concave and convex sides of the hottest fuel plate node at the time of the peak temperature. This causes a serious reduction in the heat transfer coefficient on the plate node surfaces, as shown in the middle panel, which is due to the boiling regimes at the node surfaces, as shown in the bottom panel. Page 4-75 of Volume IV of the RELAP5-3D manual [16] defines heat transfer modes 2 through 6 as the following, which was copied verbatim from the manual:

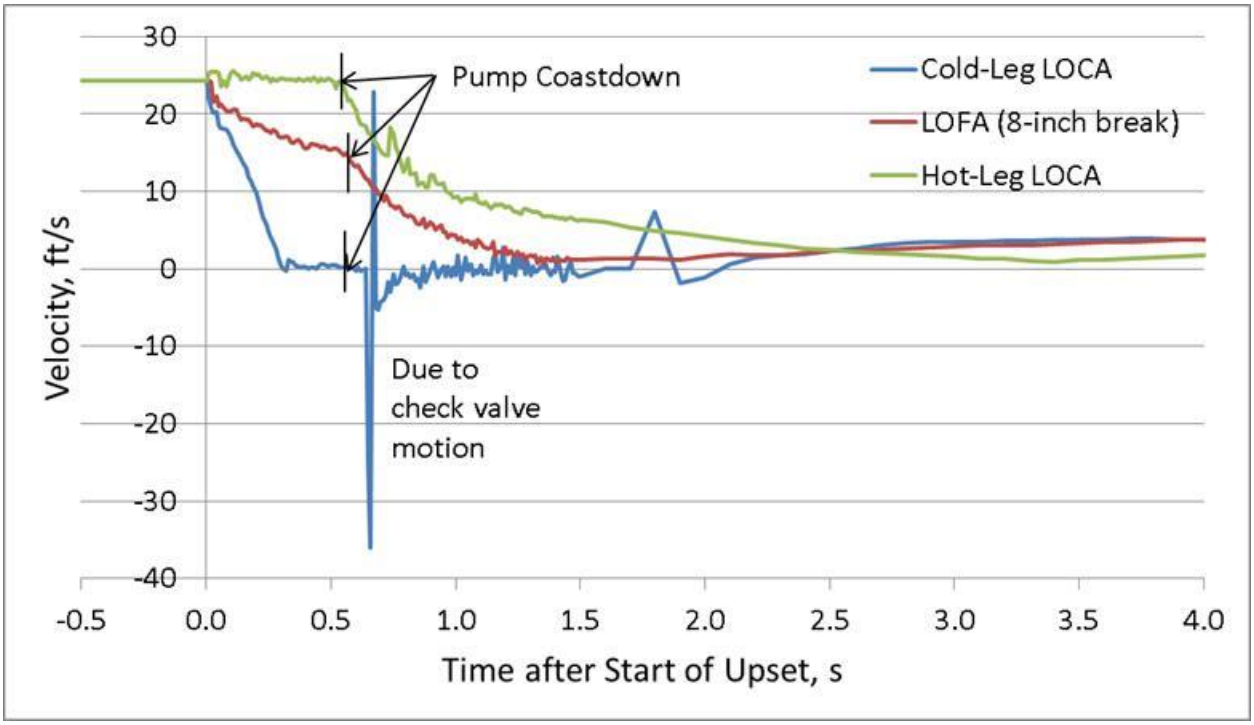

Figure 3.16. HEU Velocity in Channel 2 (between Plates 1 and 2).

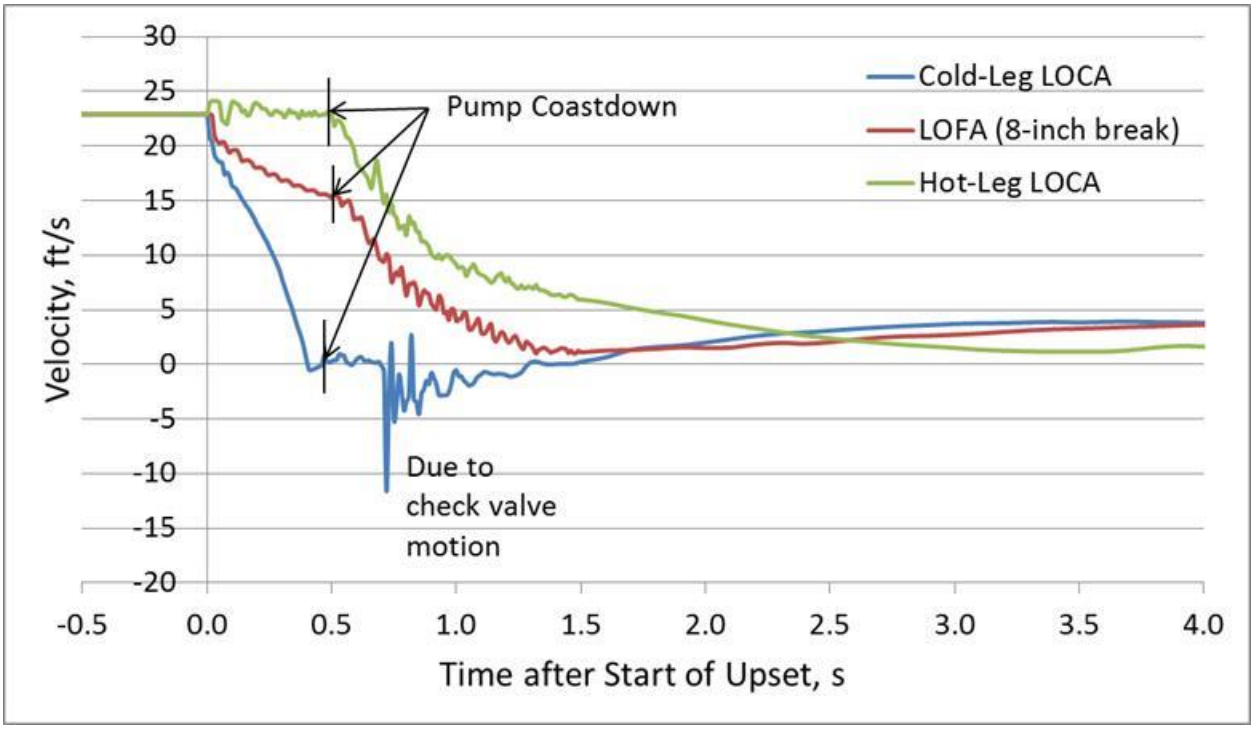

Figure 3.17. LEU Velocity in Channel 23 (between Plates 22 and 23).

"Mode 2 Single-phase liquid convection at subcritical pressure, subcooled wall and low void fraction.

Mode 3 Subcooled nucleate boiling.

Mode 4 Saturated nucleate boiling.

Mode 5 Subcooled transition boiling.

Mode 6 Saturated transition boiling."

Thus, at about the time of the scram the heat transfer mode on either side of the hottest node switches from subcooled nucleate boiling to subcooled and saturated transition boiling, which accounts for the corresponding sudden reduction in heat transfer coefficient. At about 0.60 s the reduction in power caused by the scram 0.2 s earlier allows the severe voiding of the channels to subside and the heat transfer mode starts to return to subcooled nucleate boiling, which allows the heat transfer coefficient to recover and the fuel plate centerline temperature at the node to resume the decline that it started at the scram. Although the initial steady-state temperature of node 3 of plate 1 is 10.1 °F higher than that of node 3 of plate 2, in the HEU cold-leg LOCA it is node 3 of plate 2 that is limiting. This may be due to the first channel being 0.110 inches thick versus, 0.080 inches for channels 2 and 3. This causes the initial steady-state velocity for channel 1 to be 29.5 ft/s versus 24.3 ft/s for channels 2 and 3. The greater velocity and flow rate of channel 1 coupled with the heat loss through the convex inner vessel wall surface that bounds channel 1 helps to reduce the tendency to produce voids in channel 1, which in turn allows the heat transfer on the concave side of plate 1 to remain in heat transfer mode 2 or 3 throughout the first second of the cold-leg LOCA transient. Both sides of node 3 of plate 2 are in mode 5 or 6 from 0.40 to 0.60 s. This may be the cause of the limiting location occurring in plate 2 instead of plate 1.

For the most severe LEU accident, the cold-leg LOCA, the heat transfer mode on both surfaces of the limiting node, axial node 3 of plate 23, was examined over the entire 2500-s transient, in order to verify that there was no long term temperature excursion after the initial peak. After less than 20 minutes both surfaces are in mode 2, which corresponds to single-phase flow and subcooled temperatures on the heated surfaces. The in-pool heat exchanger is not expected to function during a LOCA due to loss of coolant causing no primary coolant in the in-pool primary system above the top of the pressure vessel. The model behaved as expected, with the void fraction at the highest point in the top of the in-pool heat exchanger reaching a void fraction of 1.00 prior to 10 s into the transient and remaining constant at essentially 1.00 thereafter. At about the same time the flow rate through the in-pool heat exchanger goes to zero and remains near zero with a small random oscillation whose amplitude is in the range of ±0.02 lbm/s. This amplitude is to be compared with full reactor flow of about 520 lbm/s. The random period of this oscillation varies in the range of about 1 to 3 s. Concurrent small oscillations are also evident in the coolant and fuel plate temperatures and the pressures. Though small, the cause of the oscillations should be investigated further in the future.

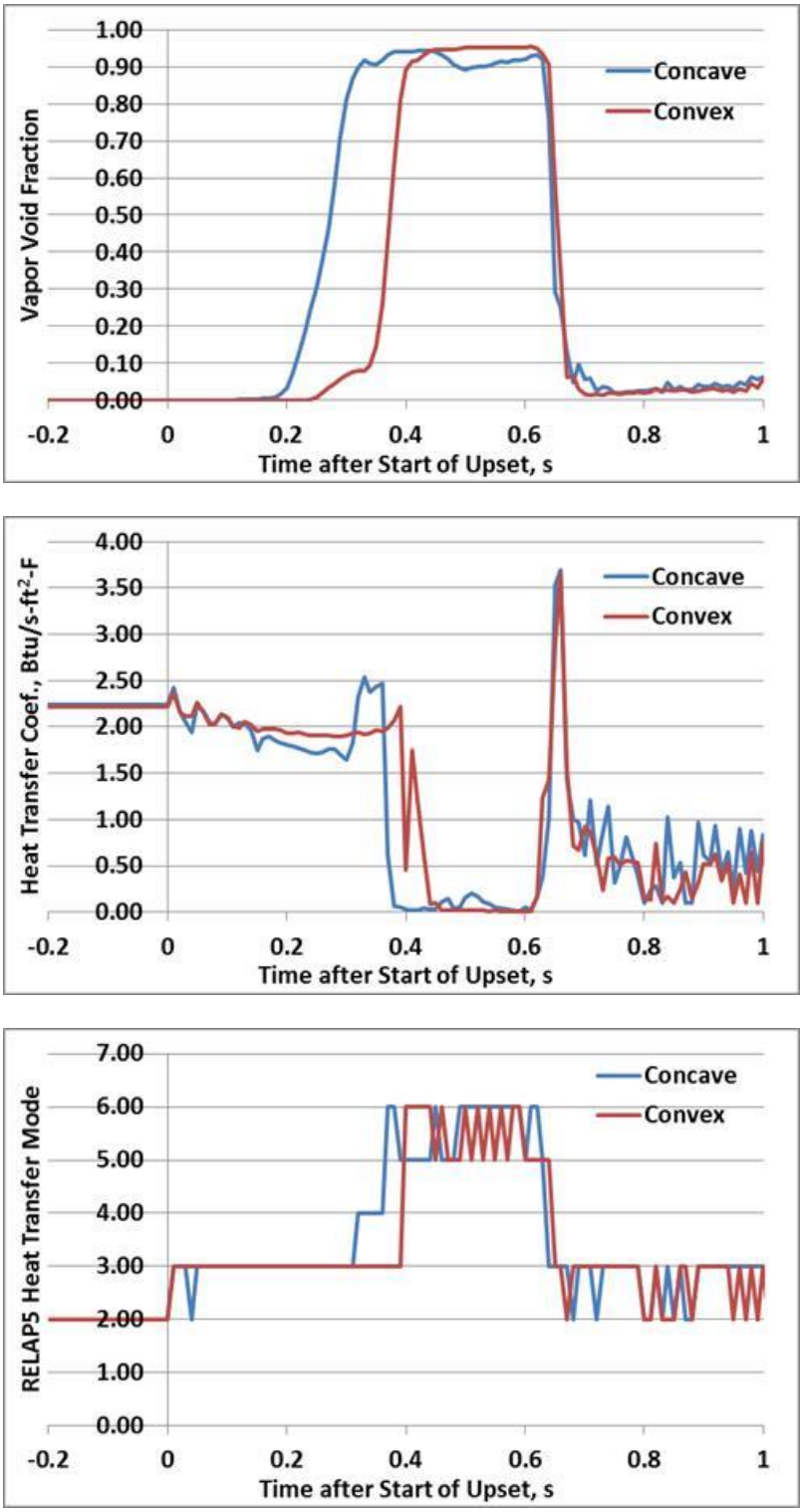

Figure 3.18. Coolant and Heat Transfer Conditions at the Limiting HEU Cold-Leg LOCA Node (Plate 2, Node 3).

3.5 Discussion

For the HEU core, given the substantial differences in hydraulic parameters between the current and the SAR analyses, some differences in the distribution of the steady-state fuel plate temperatures at full power are to be expected. Hence, with regard to comparing old and new HEU fuel plate temperatures, it is best to focus on the maximum transient rise in fuel plate temperature at a limiting location rather than the value of the peak temperature. Table 3.2 provides key temperature results for the current analysis and the corresponding results from the MURR SAR. As expected in both the SAR results and the current HEU results, the highest fuel centerline temperature occurs in the cold-leg LOCA. In the SAR results, the maximum fuel centerline temperature of 311.7 °F is 68.1 °F above the initial steady-state value for the same fuel plate node, which is node 4 of plate 3. In the current HEU analysis the maximum is 341.5 °F and is 97.2 °F above the initial steady-state value for the same fuel plate node, which is node 3 of plate 2. These peak values follow the double-end break by a few tenths of a second. The second full paragraph of page 13.29 of the MURR SAR indicates that the rods start to drop at 0.167 s. In the current analysis this occurs at 0.411 s. Given how fast temperatures rise prior to the scram and the differences in the timing of the scram, these differences in temperature rise are reasonable.

The larger HEU temperature rise in the LOFA for the current analysis versus the SAR analysis, 18.3 versus 8.2 °F, is reasonable given that the current analysis is for a large-break and the SAR analysis is for a small break.

The lack of HEU temperature rise in the hot-leg LOCA for the current analysis versus the 9.1 °F temperature rise in the SAR analysis is probably due to a difference in flow rate predicted to occur before the control rods begin to drop. The current analysis predicts no flow decrease prior to the rod motion, while the SAR analysis predicted a decrease, as indicated in the first full paragraph on page 13-36 of the MURR SAR. The cause of the drop in flow in the SAR analysis was due to modeling less time delay in tripping the primary pumps off.

As Figure 3.13 shows, in the full-power steady-state solution for the LEU core the highest fuel centerline temperature, 311.0 °F, is clearly in node 3 of plate 23. The next highest fuel node temperature, 292.7 °F, is 18.3 °F lower and is in node 3 of plate 22. Thus, it is reasonable that in all three transients node 3 of plate 23 is the limiting location. The increase in peak temperature due to the pipe rupture is greatest in the cold-leg LOCA at 35.5 °F. It is 12.5 °F in the large-break LOFA and 0.0 °F in the hot-leg LOCA.

The current analysis was done on an essentially nominal basis without uncertainty factors and without power peaking factors to account for variations in power along the arc length of each fuel plate. A way to include these considerations into the safety analysis of severe accidents would be to add the transient fuel meat temperature rises, to the corresponding values obtained from a steady-state analysis that includes uncertainty factors and power variations along the fuel plate arc length. In this regard, the very low LEU peak-location temperature rise of 35.5 °F (19.7 °C) for the worst-case depressurization accident, the cold-leg LOCA, is encouraging.

Furthermore, the axial discretization of the power profile may need to be refined to better predict the peak fuel temperature.

As indicated in Table 3.2, in the current analysis, the transient temperature rise for the cold-leg LOCA is much greater for the HEU core than for the LEU core, 97.2 versus 35.5 °F, in spite of greater power for the LEU core – 12.60 MW versus 10.38 MW for the HEU core – but essentially the same flow rate. The highest two steady-state temperatures in the LEU cold-leg LOCA occur in the third node of plates 22 and 23, during the first second of the transient. The void fraction in the common coolant node between these two hottest fuel plate nodes rapidly increases from 0 at about 0.3 s to a peak of over 0.9 at about 0.45 s

and doesn't drop below 0.8 until about 0.7 s where it rapidly returns to 0 by about 0.75 s. During this time in the interval between 0.3 and 0.75 s the void fractions of the opposite sides of the two fuel plate nodes are 0 most of the time and relatively small the rest the time. Thus, while the high void fraction temporarily impedes the heat transfer on one side of each fuel plate node, at the same time there is good heat transfer on the opposite faces. Hence, the delayed and increased peak fuel temperature that is exhibited by the HEU core, Figure 3.14, during the cold-leg LOCA doesn't appear in the LEU core, Figure 3.15.

Since in all cases considered, the peak fuel temperature always occurs within the first second of the transient, it is reasonable for the first phase of this analytical effort to focus on the first four seconds of the transients. This enabled the phenomena that led to the peak temperatures to be more closely examined. However, an important aspect of the transient behavior is the long-term heat removal. The in-pool heat exchanger is not expected to function during a LOCA due to gas stratification in the primary system. Thus, long-term cooling must be accomplished by heat transfer through the inner and outer vessel walls where they are adjacent to the first or last fuel plates and through the inner and outer vessel walls in the upper plenum. This heat transfer is facilitated by the pool-loop flow along these walls. Also, heat must be transferred from the coolant channels that are not adjacent to these walls. This heat transfer is primarily circulation among the core coolant channels with upward flow in the higher temperature coolant channels and downward flow in the cooler channels. If the long-term heat removal were not adequate, the temperatures within the core could rise over time instead of decline as the decay power gradually decreases.

Since the modeling considered only the highest heat flux element of a fresh HEU core and the corresponding element of the LEU core, future analysis may need to be expanded to include at least other LEU core cases prescribed in the neutron physics analysis [1]. Consideration must also be given to whether including only a single element in the RELAP5 model is sufficient. A major consideration in this regard is the amount of interaction between elements that can be expected and how such interaction could affect the peak temperature. This interaction is likely to occur when fresh and highly burned elements are present in the same core. The narrowing of the channels of the burned elements, due to oxidation and swelling, could divert flow to the fresh elements. Careful reasoning here with regard to the mechanisms that cause fuel temperatures to rise during the transient may prove sufficient to obviate the need to add more elements to the model and substantially increase the size and complexity of an already large and complex model.

3.6 Conclusions

The substantial RELAP5 model in the MURR SAR has been examined in detail. Improvements were made as part of the current analysis which include revising the reactor trip and protection system model; improving detail of the hydraulic parameters of the HEU core model; and reducing the thermal conductivity of the HEU fuel meat to about 55% of its original values. Also, a secondary side was added to the primary loop and pool loop heat exchangers. The improved HEU model was used to produce a single unified model which was used to model all three LOCA and LOFA upsets for the HEU core. A single large input file contains the entire steady-state model for the HEU core. A very short restart input file was produced for each transient. The power generation values of the 96 fuel meat nodes, i.e., 24 fuel plate × 4 axial level nodes, were set to represent the full power of element 7 of the HEU core power distribution 1B1, as provided by the neutron physics analysis [1]. This element has the highest heat flux in core 1B1, which is a fresh core. Since in effect the RELAP5 model has eight copies of this model, the total system power is 11.04 MW instead of 10.00.

Once the unified HEU model was complete, it was used to produce a unified model for the LEU core. This required transforming the HEU core model into an LEU one. The last coolant channel and fuel plate

were eliminated since the LEU core has 23 plates and 24 coolant channel instead of the 24 plates and 25 channels of the HEU core. The specific coolant channel gap thicknesses, aluminum clad layer, zirconium clad layer, and fuel meat thicknesses of the fresh LEU core were explicitly represented. Analogous to the new HEU core model, the LEU core fuel foil power values were set to represent element 6 of core 5B1, a fresh core, as provided by neutron physics analysis [1]. In the model the total system power was 13.07 MW instead of 12.00.

A steady-state solution was obtained for the HEU unified model and another was obtained for the LEU one. Each of these served as the initial condition for all three depressurization transients – the cold-leg LOCA, the rupture of the 540 diaphragm valve, and the hot-leg LOCA. HEU key results for each transient were compared with their LEU counterparts and with their MURR SAR counterparts, Table 3.2. In all cases the peak fuel centerline temperature occurs at the scram or a few tenths of a second after it, and always occurs during the first second of the transient. In both HEU sets of cases and the LEU set, the transient that produced the greatest fuel centerline temperature is the cold-leg LOCA.

The SAR shows that the cold-leg LOCA causes the HEU fuel node that produces the highest temperature has a fuel meat temperature rise of 68 °F (38 °C), which is to be compared with the 97 °F (54 °C) temperature rise in the HEU core predicted by the current analysis. For LEU core, the current model predicts the corresponding temperature rise to be only 36 °F (20 °C). This is a very modest temperature rise for such a severe accident. The peak fuel temperature during the cold-leg LOCA is predicted to be 342 °F (172 °C) for the HEU and 347 °F (175 °C) for the LEU.

Important aspects of the analysis, such as long-term cooling of the core, were considered in the SAR analysis, but only in a cursory manner in this new scoping analysis. Only fresh elements were modeled. The core model is only one element that is scaled up to represent all eight. Since the pressurizer level is not modeled, it was assumed in the current analysis that the 527C valve, which is between the pressurizer and the main primary coolant loop, closes at the initiation of each transient. These are areas for possible further investigation in Phase II of the analysis.

In conclusion, the preliminary results of this report indicate acceptable thermal performance for the LEU core and a reasonable comparison between the current and the MURR SAR results for the HEU core.

4.0 CONCLUSIONS

Safety analyses of the MURR core fueled with a monolithic alloy of uranium and 10 wt% molybdenum (U-10Mo) were previously conducted to establish the steady-state safety basis of the reactor using the CD35 fuel element design [1, 5]. The thermal-hydraulic analyses of the reactor required detailed power distributions and geometrical considerations in order to identify regions of interest for safety analyses. In order to understand the impacts of accident and transient scenarios in a core fueled with an LEU U-10Mo element, a set of preliminary accident analyses have been performed. NUREG-1537 guidelines [7] postulate nine classes of postulated accident-initiating scenarios. The preliminary analyses include evaluation of those which have been the most challenging to fuel integrity including reactivity insertion accidents, loss of coolant accidents, and a loss of flow accident. The objective of these preliminary analyses was to determine the range of conditions and temperatures that the fuel, which is under development, should be expected to experience under off-normal and other transient scenarios.

Accidents resulting from the uncontrolled or unanticipated insertion of positive reactivity in the MURR core have been evaluated to assess the impact of fuel conversion on the reactor safety. First, several positive step reactivity insertions, based upon the various maximum reactivity limits given in the MURR Technical Specifications were considered. Second, a continuous ramp insertion of positive reactivity based on the simultaneous continuous withdrawal of MURR's four shim control blades was considered. The exact mechanisms or events that could cause these reactivity insertions can vary, but could include an inadvertent rapid insertion or removal of an experiment from the center test hole, reactor or equipment malfunction, or operator error. The reactivity insertion transient analyses were performed using the PARET/ANL (V. 7.5) code [3].

For the most limiting reactivity insertion accident, which is a 0.006 $\Delta k/k$ step insertion of reactivity in a fresh critical core at full power, the peak HEU U-Al_x fuel meat temperature is calculated to be 444 ^oF (229 ^oC). The same accident is also the most limiting for the LEU fuel, resulting in a peak U-10Mo temperature of 500 ^oF (260 ^oC). The HEU analyses were for 10 MW initial steady-state power, while the LEU analyses were for 12 MW initial steady-state power. In both cases, the fuel temperature is well below the measured fuel blister threshold temperatures of 896 ^oF (480 ^oC) and 752 ^oF (400 ^oC) for HEU and LEU fuel, respectively.

Accidents resulting from cooling system failure were analyzed by a RELAP5 [6] model in order to assess the impact of fuel conversion on the reactor safety. After review of potential accidents, consistent with NUREG-1537, the following three depressurization accidents were analyzed for both an HEU core and an LEU core:

1. Cold-leg LOCA – double-end 12-inch diameter break at the core side of the 507B cold-leg isolation valve.
2. Hot-leg LOCA – double-end 12-inch diameter break at the core side of the 507A hot-leg isolation valve.
3. LOFA – 8-inch diameter breach in the 8-inch cold-leg piping at the flow control diaphragm valve.

For the limiting cooling system failure accident, the cold-leg LOCA, the peak HEU fuel temperature during the LOCA is predicted to be 342 °F (172 °C). For the LEU core peak LEU fuel temperature during the LOCA is predicted to be 347 °F (175 °C). The HEU analyses were for 10 MW initial steady-state power, while the LEU analyses were for 12 MW initial steady-state power.

The preliminary results provided herein indicate acceptable thermal performance for the LEU core at 12 MW, and a reasonable comparison between the current and the MURR SAR results for the HEU core at 10 MW.

The analyses reported herein represent Phase I of a two-phased effort to develop the complete Chapter 13 for an LEU Conversion SAR.

The Phase I analyses considered limiting core power distributions, but focused on the thermal performance of the peak heat flux plates. Those plates were fresh. Subsequent Phase II analyses will assess the impact of fuel swelling due to burnup, oxide layer growth, and the associated restriction of the coolant channel. Depleted plates have lower power than fresh plates in the MURR core (due to depletion), but could experience similar or even higher temperatures than fresh plates during accidents due to the degradation of heat transfer. Phase II analyses will also assess the importance of fabrication tolerances and of uncertainties in fuel properties and initial conditions (flow, power, etc.). While the Phase I analyses did treat the increase in potential power peaking due to control blade depletion, the impact of control rod depletion on accidents due to reduced SCRAM worth will be evaluated in Phase II. Finally, additional improvement of the PARET/ANL and RELAP5 models will be considered in Phase II in order to reduce unnecessary conservatisms where appropriate.

REFERENCES

1. J. Stillman, et al., *Technical Basis in Support of the Conversion of the University of Missouri Research Reactor (MURR) Core from High-Enriched to Low-Enriched Uranium – Core Neutron Physics*, ANL/RERTR/TM-12-30, Argonne National Laboratory, September 2012.

2. *University of Missouri Research Reactor Safety Analysis Report*, submitted to the U.S. Nuclear Regulatory Commission in 2006.

3. A. P. Olson, *A Users Guide to the PARET/ANL Code, Version 7.5*, ANL/RERTR/TM-11-38, Version 7.5, August 14, 2012.

4. X-5 Monte Carlo Team, "MCNP-A General Monte Carlo N-Particle Transport Code, Version 5 Volume I, II and III," LA-UR-03-1987/LA-CP-03-0245/LA-CP-03-0284, Los Alamos National Laboratory (2003).

5. Feldman, E. E., et al., *Technical Basis in Support of the Conversion of the University of Missouri Research Reactor (MURR) Core from Highly-Enriched to Low-Enriched Uranium – Steady-State Thermal-Hydraulic Analysis*, ANL/RERTR/TM-12-37, Argonne National Laboratory, August 2012.

6. "RELAP5/MOD3.3 Code Manual," NUREG/CR-5535/Rev 1, Information Systems Laboratories, Inc., Rockville, MD and Idaho Falls, ID, December 2001.

7. *Guidelines for Preparing and Reviewing Applications for the Licensing of Non-Power Reactors, Standard Format and Content*, NUREG-1537, Part 1, February 1996.

8. D. E. Burkes, G. S. Mickum, and D. M. Wachs, *Thermophysical Properties of U-10Mo Alloy*, INL/EXT-10-19373, November 2010, Idaho National Laboratory, http://www.inl.gov/technicalpublications/Documents/4702554.pdf.

9. J.G. Crocker, and L.A. Stephan, *Reactor Power Excursion Tests in the SPERT IV Facility*, AEC Research and Development Report, IDO-17000, August 1964.

10. J. M. Beeston, R. R. Hobbins, G. W. Gibson, and W. C. Francis, "Development and Irradiation of Uranium Aluminide Fuels in Test Reactors," *Nucl. Tech*., Vol. 49, p. 136-149 (June 1980).

11. F. Rice, et al., "GTRI Blister Anneal and Fission Product Testing," U.S. High Performance Research Reactor Working Group Meeting, Los Alamos, New Mexico, June 11-13, 2013.

12. Sadic Kakac, Ramesh K. Shah, Win Aung, *Handbook of Single-Phase Convective Heat Transfer*, John Wiley and Sons, New York, 1987.

13. J. E. Matos and J. L. Snelgrove, "Selected Thermal Properties and Uranium Density Relations for Alloy, Aluminide, Oxide, and Silicide Fuel," *Research Reactor Core Conversion Guidebook*, IAEATECDOC-643, Volume 4: Fuels Appendices I-1.1, IAEA, Vienna, Austria, 1992, pp. 13-29.

14. J. K. Fink and L. Leibowitz, "Thermal Conductivity of Zirconium," *Journal of Materials*, 226 (1995) 44-50.

15. Symbolic Nuclear Analysis Package (SNAP) User's Manual, Version 2.2.1 – October 25, 2012, Applied Programming Technology, Inc., Bloomsburg, PA, 2012.

16. The RELAP5-3D© Code Development Team, *RELAP5-3D© Code Manual*, Revision 4.0, INEEL-EXT-98-00834, Idaho National Laboratory, June 2012.

Appendix A: Tables of Key HEU and LEU Core Parameter Data

Table A.1. HEU Core Coolant Channel Hydraulic Diameters, Shape Factors, and 8 × Flow Areas.

Channel number	Inner radius, in.	Outer radius, in.	Hydraulic diameter, ft.	Aspect ratio	Shape factor, Φs	8 × Flow Area, feet^2
1	2.660	2.770	0.01727	0.0614	0.722	1.095E-02
2	2.820	2.900	0.01280	0.0420	0.704	8.472E-03
3	2.950	3.030	0.01282	0.0398	0.702	8.926E-03
4	3.080	3.160	0.01285	0.0379	0.701	9.380E-03
5	3.210	3.290	0.01287	0.0362	0.699	9.834E-03
6	3.340	3.420	0.01289	0.0346	0.698	1.029E-02
7	3.470	3.550	0.01291	0.0331	0.696	1.074E-02
8	3.600	3.680	0.01292	0.0318	0.695	1.119E-02
9	3.730	3.810	0.01294	0.0305	0.694	1.165E-02
10	3.860	3.940	0.01295	0.0294	0.693	1.210E-02
11	3.990	4.070	0.01297	0.0283	0.692	1.256E-02
12	4.120	4.200	0.01298	0.0273	0.691	1.301E-02
13	4.250	4.330	0.01299	0.0264	0.690	1.346E-02
14	4.380	4.460	0.01300	0.0255	0.690	1.392E-02
15	4.510	4.590	0.01301	0.0247	0.689	1.437E-02
16	4.640	4.720	0.01302	0.0240	0.688	1.483E-02
17	4.770	4.850	0.01303	0.0233	0.688	1.528E-02
18	4.900	4.980	0.01304	0.0226	0.687	1.573E-02
19	5.030	5.110	0.01305	0.0220	0.686	1.619E-02
20	5.160	5.240	0.01305	0.0214	0.686	1.664E-02
21	5.290	5.370	0.01306	0.0208	0.685	1.709E-02
22	5.420	5.500	0.01307	0.0203	0.685	1.755E-02
23	5.550	5.630	0.01308	0.0198	0.684	1.800E-02
24	5.680	5.760	0.01308	0.0193	0.684	1.846E-02
25	5.810	5.900	0.01469	0.0211	0.686	2.129E-02

Table A.2. LEU Core Coolant Channel Hydraulic Diameters, Shape Factors, and 8 × Flow Areas.

Channel number	Inner radius, in.	Outer radius, in.	Hydraulic diameter, ft.	Aspect ratio	Shape factor, Φs	8 × Flow Area, feet^2
1	2.660	2.756	0.01511	0.0535	0.715	9.479E-03
2	2.7995	2.8925	0.01477	0.0491	0.711	9.792E-03
3	2.9365	3.0295	0.01481	0.0464	0.708	1.035E-02
4	3.0735	3.1665	0.01485	0.0441	0.706	1.090E-02
5	3.2105	3.3035	0.01488	0.0419	0.704	1.146E-02
6	3.3475	3.4395	0.01475	0.0396	0.702	1.188E-02
7	3.4835	3.5755	0.01477	0.0378	0.701	1.243E-02
8	3.6195	3.7115	0.01480	0.0362	0.699	1.298E-02
9	3.7555	3.8475	0.01482	0.0348	0.698	1.352E-02
10	3.8915	3.9835	0.01484	0.0334	0.697	1.407E-02
11	4.0275	4.1195	0.01486	0.0322	0.696	1.461E-02
12	4.1635	4.2555	0.01487	0.0310	0.695	1.516E-02
13	4.2995	4.3915	0.01489	0.0299	0.694	1.571E-02
14	4.4355	4.5275	0.01490	0.0289	0.693	1.625E-02
15	4.5715	4.6635	0.01492	0.0280	0.692	1.680E-02
16	4.7075	4.7995	0.01493	0.0271	0.691	1.734E-02
17	4.8435	4.9355	0.01494	0.0263	0.690	1.789E-02
18	4.9795	5.0715	0.01495	0.0255	0.690	1.844E-02
19	5.1155	5.2075	0.01496	0.0248	0.689	1.898E-02
20	5.2515	5.3445	0.01513	0.0243	0.689	1.974E-02
21	5.3885	5.4815	0.01514	0.0237	0.688	2.030E-02
22	5.5255	5.6185	0.01515	0.0230	0.687	2.085E-02
23	5.6625	5.7555	0.01516	0.0224	0.687	2.141E-02
24	5.8045	5.900	0.01557	0.0224	0.687	2.258E-02

Table A.3. HEU Fuel Plate Heat Transfer Areas for Flat-Plate (Rectangular) Geometry.

	Radius, inches			Avg. Heated Perimeter, inches	Heat Transfer Area, feet^2		8 × Heat Transfer Area, feet^2	
Plate	inner	outer	average		7.75-inch nodes	5.00-inch nodes	7.75-inch nodes	5.00-inch nodes
1	2.770	2.820	2.795	1.703	0.0917	0.0591	0.7333	0.4731
2	2.900	2.950	2.925	1.805	0.0972	0.0627	0.7773	0.5015
3	3.030	3.080	3.055	1.907	0.1027	0.0662	0.8212	0.5298
4	3.160	3.210	3.185	2.009	0.1081	0.0698	0.8652	0.5582
5	3.290	3.340	3.315	2.112	0.1136	0.0733	0.9092	0.5866
6	3.420	3.470	3.445	2.214	0.1191	0.0769	0.9531	0.6149
7	3.550	3.600	3.575	2.316	0.1246	0.0804	0.9971	0.6433
8	3.680	3.730	3.705	2.418	0.1301	0.0840	1.0410	0.6716
9	3.810	3.860	3.835	2.520	0.1356	0.0875	1.0850	0.7000
10	3.940	3.990	3.965	2.622	0.1411	0.0910	1.1290	0.7284
11	4.070	4.120	4.095	2.724	0.1466	0.0946	1.1729	0.7567
12	4.200	4.250	4.225	2.826	0.1521	0.0981	1.2169	0.7851
13	4.330	4.380	4.355	2.928	0.1576	0.1017	1.2608	0.8134
14	4.460	4.510	4.485	3.031	0.1631	0.1052	1.3048	0.8418
15	4.590	4.640	4.615	3.133	0.1686	0.1088	1.3488	0.8702
16	4.720	4.770	4.745	3.235	0.1741	0.1123	1.3927	0.8985
17	4.850	4.900	4.875	3.337	0.1796	0.1159	1.4367	0.9269
18	4.980	5.030	5.005	3.439	0.1851	0.1194	1.4806	0.9553
19	5.110	5.160	5.135	3.541	0.1906	0.1230	1.5246	0.9836
20	5.240	5.290	5.265	3.643	0.1961	0.1265	1.5686	1.0120
21	5.370	5.420	5.395	3.745	0.2016	0.1300	1.6125	1.0403
22	5.500	5.550	5.525	3.847	0.2071	0.1336	1.6565	1.0687
23	5.630	5.680	5.655	3.949	0.2126	0.1371	1.7004	1.0971
24	5.760	5.810	5.785	4.052	0.2181	0.1407	1.7444	1.1254

Table A.4. LEU Fuel Plate Heat Transfer Areas for Flat-Plate (Rectangular) Geometry.

	Radius, inches			Avg. Heated Perimeter, inches	Heat Transfer Area, feet^2		8 × Heat Transfer Area, feet^2	
Plate	inner	outer	average		7.75-inch nodes	5.00-inch nodes	7.75-inch nodes	5.00-inch nodes
1	2.756	2.800	2.778	1.689	0.0909	0.0587	0.7274	0.4693
2	2.893	2.937	2.915	1.797	0.0967	0.0624	0.7737	0.4992
3	3.030	3.074	3.052	1.905	0.1025	0.0661	0.8201	0.5291
4	3.167	3.211	3.189	2.012	0.1083	0.0699	0.8664	0.5590
5	3.304	3.348	3.326	2.120	0.1141	0.0736	0.9127	0.5888
6	3.440	3.484	3.462	2.227	0.1198	0.0773	0.9587	0.6185
7	3.576	3.620	3.598	2.333	0.1256	0.0810	1.0047	0.6482
8	3.712	3.756	3.734	2.440	0.1313	0.0847	1.0507	0.6779
9	3.848	3.892	3.870	2.547	0.1371	0.0884	1.0967	0.7075
10	3.984	4.028	4.006	2.654	0.1428	0.0921	1.1427	0.7372
11	4.120	4.164	4.142	2.761	0.1486	0.0959	1.1886	0.7669
12	4.256	4.300	4.278	2.868	0.1543	0.0996	1.2346	0.7965
13	4.392	4.436	4.414	2.974	0.1601	0.1033	1.2806	0.8262
14	4.528	4.572	4.550	3.081	0.1658	0.1070	1.3266	0.8559
15	4.664	4.708	4.686	3.188	0.1716	0.1107	1.3726	0.8856
16	4.800	4.844	4.822	3.295	0.1773	0.1144	1.4186	0.9152
17	4.936	4.980	4.958	3.402	0.1831	0.1181	1.4646	0.9449
18	5.072	5.115	5.094	3.508	0.1888	0.1218	1.5106	0.9746
19	5.207	5.251	5.229	3.615	0.1946	0.1255	1.5566	1.0042
20	5.344	5.388	5.366	3.723	0.2004	0.1293	1.6029	1.0341
21	5.481	5.525	5.503	3.830	0.2062	0.1330	1.6492	1.0640
22	5.618	5.662	5.640	3.938	0.2119	0.1367	1.6955	1.0939
23	5.755	5.804	5.780	4.048	0.2178	0.1405	1.7427	1.1243

Table A.5. Thermal Properties in MURR RELAP5 Models.

Material 1 (Aluminum Walls & HEU Clad)					
Temperature		Thermal Conductivity		Heat Capacitance	
^oF	^oC	Btu/s-ft-^oF	W/m-^oC	Btu/ft^3-^oF	kJ/m^3-^oC
68	20.0	0.02689	167.5	37.86	2539
500	260.0	0.02958	184.3	40.08	2688
1000	537.8	0.03227	201.1	42.17	2828
3000	1648.9	0.04303	268.1	50.56	3391

Material 2 (HEU Dispersion Fuel Meat)							
		MURR SAR Model		Current RELAP5 Model		Both HEU Models	
Temperature		Thermal Conductivity		Thermal Conductivity		Heat Capacitance	
^oF	^oC	Btu/s-ft-^oF	W/m-^oC	Btu/s-ft-^oF	W/m-^oC	Btu/ft^3-^oF	kJ/m^3-^oC
68	20.0	0.01194	74.39	0.00642	40.0	33.50	2247
500	260.0	0.01144	71.28	0.00642	40.0	35.60	2388
1000	537.8	0.01094	68.16	0.00642	40.0	38.17	2560
3000	1648.9	8.940E-03	55.70	0.00642	40.0	48.46	3250

Material 3 (Aluminum of Piping and In-Pool Heat Exchanger					
Temperature		Thermal Conductivity		Heat Capacitance	
^oF	^oC	Btu/s-ft-^oF	W/m-^oC	Btu/ft^3-^oF	kJ/m^3-^oC
68	20.0	0.03222	200.8	37.86	2539
500	260.0	0.03383	210.8	40.08	2688
1000	537.8	0.03544	220.8	42.17	2828
3000	1648.9	0.04188	260.9	50.56	3391

Material 4 (Zirconium in LEU Clad)							
Temperature		Thermal Conductivity		Temperature		Heat Capacitance	
^oF	^oC	Btu/s-ft-^oF	W/m-^oC	^oF	^oC	Btu/ft^3-^oF	kJ/m^3-^oC
68.0	20.0	3.43E-03	21.4	68	20.0	27.83	1866
200.0	93.3	3.20E-03	20.0	400	204.4	30.11	2019
400.0	204.4	3.06E-03	19.1	1000	537.8	33.46	2244
531.3	277.4	3.04E-03	19.0	2000	1093.3	38.76	2599
700.0	371.1	3.07E-03	19.1	3000	1648.9	44.00	2951
1000.0	537.8	3.20E-03	20.0				
2000.0	1093.3	4.09E-03	25.5				
3000.0	1648.9	5.36E-03	33.4				

Table A.5 (cont'd). Thermal Properties in Original MURR RELAP5 Model.

Material 5 (Unirradiated U-10Mo LEU Fuel Foil)							
Temperature		Thermal Conductivity		Temperature		Heat Capacitance	
^oF	^oC	Btu/s-ft-^oF	W/m-^oC	^oF	^oC	Btu/ft^3-^oF	kJ/m^3-^oC
68	20.0	1.75E-03	10.9	68	20.0	35.23	2363
3000	1648.9	1.09E-02	68.1	200	93.3	36.23	2430
				400	204.4	37.85	2538
				600	315.6	39.59	2655
				800	426.7	41.46	2781
				1000	537.8	43.46	2915
				2000	1093.3	55.32	3710
				3000	1648.9	70.32	4716

Nuclear Engineering Division
Argonne National Laboratory
9700 South Cass Avenue, Bldg. 208
Argonne, IL 60439

www.anl.gov

Argonne National Laboratory is a U.S. Department of Energy
laboratory managed by UChicago Argonne, LLC